SEARCHING FOR HEAVY PHOTONS WITH DETACHED VERTICES IN THE HEAVY PHOTON SEARCH EXPERIMENT

by

Holly Szumila-Vance
B.S. May 2008, Embry-Riddle Aeronautical University
B.S. May 2009, Embry-Riddle Aeronautical University
M.S. May 2014, Old Dominion University

A Dissertation Submitted to the Faculty of
Old Dominion University in Partial Fulfillment of the
Requirements for the Degree of

DOCTOR OF PHILOSOPHY

PHYSICS

OLD DOMINION UNIVERSITY
June 2017

Approved by:

Lawrence Weinstein (Director)

John Adam (Member)

J. W. Van Orden (Member)

Stepan Stepanyan (Member)

Leposava Vuskovic (Member)

ABSTRACT

SEARCHING FOR HEAVY PHOTONS WITH DETACHED VERTICES IN THE HEAVY PHOTON SEARCH EXPERIMENT

Holly Szumila-Vance
Old Dominion University, 2017
Director: Dr. Lawrence Weinstein

The Jefferson Lab Heavy Photon Search (HPS) experiment is searching for a hypothetical massive particle called the heavy photon which could mediate a dark electromagnetic-type force. If heavy photons kinetically mix with Standard Model photons, they may be radiated by electrons scattering from a heavy nucleus and then decay to e^+e^- pairs. HPS uniquely searches for heavy photons that either decay at the target or a measurable distance after. The experiment utilizes a silicon vertex tracker (SVT) for momentum and vertex reconstruction, together with an electromagnetic calorimeter for measuring particle energies and triggering events. The HPS experiment took its first data during the spring 2015 engineering run using a 1 GeV electron beam incident on a tungsten target and its second data in the spring of 2016 at a beam energy of 2.3 GeV. The 2015 run obtained two days of production data that was used for the first physics results. The analysis of the data was conducted as a blinded analysis by tuning cuts on 10% of the data.

This dissertation discusses the displaced vertex search for heavy photons in the 2015 engineering run. It describes the theoretical motivation for looking for heavy photons and provides an overview of the HPS experimental design and performance. The performance details of the experiment are primarily derived from the 2015 engineering run with some discussion from the higher energy running in 2016.

This dissertation further discusses the cuts used to optimize the displaced vertex search and the results of the search. The displaced vertex search did not set a limit on the heavy photon but did validate the methodology for conducting the search. Finally, we used the full data set to make projections and guide future analyses.

ACKNOWLEDGMENTS

Thank you to everyone who has influenced my life and scientific development during this time. This dissertation would not have been possible without the incredible mentors and colleagues I have had the pleasure to work with. Thank to you all of my HPS collaborators for building and running a successful experiment. Thank you to the Old Dominion University Physics Department for investing so much time creating a positive and stimulating environment for budding physicists.

I would like to especially thank Larry Weinstein for being an outstanding advisor and for giving me room to explore in my research while using every opportunity to simplify and clarify new concepts. I thank Stepan Stepanyan for his guidance and direction of the HPS experiment and for organizing a supportive network at Jefferson Lab for conducting physics analysis. I also thank John Jaros for always asking questions and keeping my work relevant. Merci to Michel Garçon for teaching me the details of calorimetry as well as the value of a well-written analysis note. I thank Nathan Baltzell and Rafayel Paremuzyan for always taking the time to answer my questions and offering advice and guidance on my research. I also especially thank my collaborators at Orsay and INFN with whom I shared the exciting experience of testing and assembling a calorimeter.

And finally, I thank my family and friends for their unwavering support. I thank my father for instilling in me a curiosity for the universe and the patience needed to understand complex problems. I thank my mother for giving me the gift of communication and expression through words and the perpetual drive to always move forward. I thank my brother for his support and thoughtful discussions about life as a student and scientist- may this dissertation prove that graduate school really does eventually end, (and it is actually only the beginning).

This dissertation is dedicated to my loving husband and best friend, Jeff, for always believing in me and supporting me in everything I do.

TABLE OF CONTENTS

LIST OF TABLES

LIST OF FIGURES

CHAPTER 1

INTRODUCTION

The heavy photon, also known as the A', is a theoretically motivated massive gauge boson that is associated with a predicted U(1) hidden symmetry, favorable to Beyond Standard Model theories. According to theory [1], a heavy photon kinetically mixes with the Standard Model photon through a loop-level effect generating an effective coupling to electric charge. The relative size of this coupling to electric charge, ϵ, can range from 10^{-12} to 10^{-2} depending on the loop order of the mixing interaction and describes the coupling of the heavy photon to electric charge to be at a scale significantly smaller than that in standard electrodynamic theory. While the coupling strength of the interaction can be naturally generated from the loop interactions, the mass is somewhat less constrained. Theories of the heavy photon as a way to explain cosmological phenomena make them the simplest and possibly leading interaction between the Standard Model and the Dark Sector. The Dark Sector encompasses both dark matter and dark energy particles that do not interact other than gravitationally. If the heavy photon obtains its mass through the Higgs mechanism, the mass is favored to be in the range of MeV to GeV which is compatible with dark matter theories. In such a scenario, electrons could radiate heavy photons as they do ordinary photons but at a suppressed rate. These heavy photons will have measurable lifetimes before decaying to charged particle pairs. It is natural to describe the heavy photon parameter space in terms of its coupling, ϵ^2, and mass, $m_{A'}$.

The Heavy Photon Search (HPS) experiment is searching for heavy photons in the mass range of 20 to 1000 MeV/c^2 with prompt or displaced vertices with respect to the target interaction. HPS generates heavy photons from an electron beam incident on a heavy target and measures the momentum and vertex position of e^+e^- pairs produced from its decay. By reconstructing the invariant mass and the vertex position of the pairs, HPS can look for a small bump on a large background using a bump hunt for prompt decays. Uniquely, HPS is also able to look for heavy photons with smaller couplings (and longer lifetimes) characterized by displaced vertices by searching for a small signal on low background downstream of the target. The HPS reach attained from the 2015 engineering run from the bump hunt is shown in Figure **??** along with the existing limits from other experiments.

The HPS experiment took place in Hall B at the Jefferson Laboratory National Accelerator Facility. The Continuous Electron Beam Accelerator Facility (CEBAF) at Jefferson Lab produces an electron beam that collides with the HPS target material in Hall B. The HPS detector measures the particles from this interaction and searches for the heavy photon signal. The HPS detector consists of a Silicon Vertex Tracker (SVT) and an Electromagnetic Calorimeter (ECal). The SVT measures particle trajectories and reconstructs the vertex position of the particle pair. The ECal triggers event readout in addition to measuring particle energy and pair coincidence timing.

The ECal was commissioned during a short commissioning run in December 2014. The full experiment ran in the spring of 2015 commissioning the full beamline and both detectors. This run took 2.3 days of good data at approximately 50 nA with a beam energy of 1.056 GeV. HPS obtained a total of 1529 nb^{-1} of good data. During the commissioning of the SVT, some data was taken with the SVT slightly open from its nominal position before moving the SVT in to its designed position at ± 0.5 mm from the beam. A second run in the spring of 2016 used a 200 nA electron beam at 2.3 GeV collecting a total of 5.7 days of data. Future running at higher electron beam energy is planned for 2018 and beyond.

In this dissertation, I describe the search for heavy photons with a displaced vertex using data from the 2015 engineering run. I will describe the experiment as a whole focusing on the areas in which I was most involved. I performed a blinded analysis using 10% of the data. In order to better understand and analyze the backgrounds in the vertex search, I conducted a further study of the backgrounds using the statistics of the fully unblinded dataset. I will discuss the backgrounds and reach from the Engineering Run.

In addition to the full vertex analysis, I contributed significantly to the assembly, characterization and commissioning of the ECal for all experimental running. I wrote the clustering algorithm based on that used by the CLAS experiment Inner Calorimeter (IC) and improved simulations of the ECal detector response. I also calibrated the ECal in both energy and time for both experimental runs.

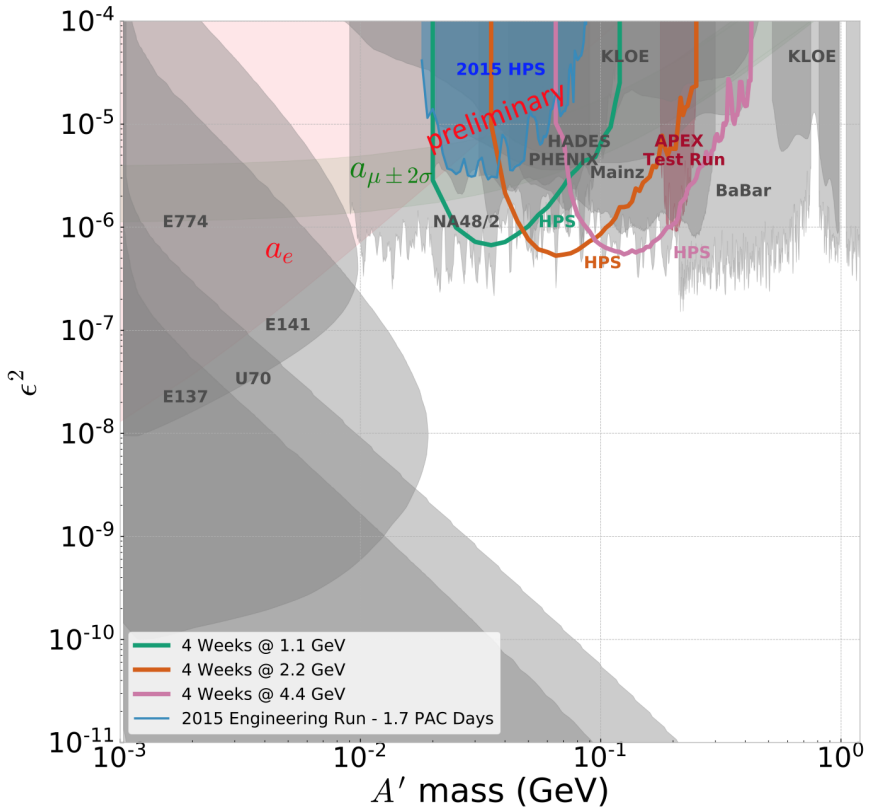

FIG. 1.0.1: The existing 90% confidence limits from other experiments looking for heavy photons in the relevant mass-coupling region is shown. The shaded blue region includes the preliminary bump hunt results from the 2015 engineering run. The vertex reach is not shown on this plot as no reach is found using the proposed HPS run configuration. The region labeled as a_μ indicates the favored parameter space for a visibly decaying heavy photon to explain the discrepancy between the calculated and measured muon anomalous magnetic moment. The experiments along the top of the plot with large coupling look for heavy photons that decay promptly at the target. The limits shown in grey along the left side of the plot with decreasing values of coupling look for heavy photons with displaced vertices in beam dump experiments.

CHAPTER 2

MOTIVATION

The Standard Model (SM) is the most successful theory for describing elementary particles and their interactions via the electromagnetic, strong, and weak forces in terms of gauge theory interactions. The existence of an additional U(1) hidden symmetry is not forbidden by the SM. The heavy photon is the proposed gauge boson for the dark electromagnetic force that would arise from a U(1) broken symmetry. If such an interaction exists, then the SM photon and heavy photon would mix, thus inducing a coupling between the heavy photon and electric charge equal to ϵe [1]. This coupling is significant because electrons could radiate heavy photons similar to radiating SM photons, although at rates decreased by ϵ^2. The primary goal of HPS and many similar experiments is to experimentally detect the heavy photon through this production mechanism. The heavy photon is additionally referred to as the A', dark photon, or U-boson.

2.1 THEORY OF HEAVY PHOTONS

The possible existence of a heavy photon rests on the allowable symmetries from the Standard Model. An additional U(1) symmetry in nature could interact with the SM through the mechanism of kinetic mixing [1]. Under kinetic mixing, a new gauge boson (heavy photon or A') couples to the electromagnetic current through the SM photon by some amount ϵ. Kinetic mixing generates the coupling strength, ϵ, through loop interactions as shown in Figure 2.1.1.

In the simplest scenario, there is one particle χ that is charged under both the U(1) and new U(1)$'$. This single loop level interaction can generate the ϵ coupling to be in the range of 10^{-4} to 10^{-2}. In Grand Unified Theory (GUT), symmetries forbid one-loop interactions and favor two-loop interactions generating an ϵ in the range of 10^{-5} to 10^{-3} [2]. If both U(1)s are in unified groups, higher loop interactions generating even smaller couplings are possible. The gauge part of the SM Lagrangian is modified to include this interaction

$$\mathcal{L}_{gauge} = -\frac{1}{4}F^{\mu\nu}F_{\mu\nu} - \frac{1}{4}F'^{\mu\nu}F'_{\mu\nu} + \frac{1}{2}\epsilon F^{\mu\nu}F'_{\mu\nu} \tag{1}$$

where $F_{\mu\nu}$ is the electromagnetic field strength tensor defined in terms of the gradient of the potential as $F_{\mu\nu} = \partial_\mu A_\nu - \partial_\nu A_\mu$, $F'_{\mu\nu}$ corresponds to the field strength of the heavy photon,

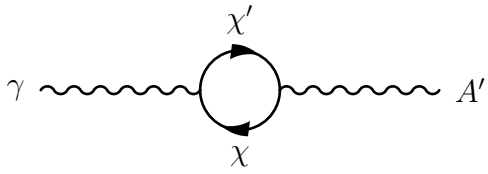

FIG. 2.1.1: Kinetic mixing of the SM photon with a heavy photon is shown at the one-loop level. χ can be any massive particle that is charged under both the A' and SM U(1) interactions.

and ϵ is the coupling. The third term of the Lagrangian is the kinetic mixing operator. The SM photon field can be re-defined as $A_\mu \rightarrow A_\mu + \epsilon A'_\mu$ to remove the kinetic mixing operator. This generates a coupling to electric charge of order ϵ seen in the interaction between the heavy photon and SM as $\epsilon e A'_\mu J^\mu_{EM}$ where J^μ_{EM} is the electromagnetic current [3]. Particles that are charged only under the A' would not acquire this fractional charge and would remain undetectable in this model.

The mass of the heavy photon is somewhat less constrained by theory. The MeV to GeV mass scale is interesting to explore because it has been generally overlooked by previous experiments and is consistent with dark matter theories that attempt to explain several astrophysical observations.

2.2 IMPLICATIONS OF A HEAVY PHOTON

The theory for the existence of the heavy photon arises from allowable symmetries of the Standard Model and can exist without other theories of dark matter. However, if the heavy photon does exist, then the interaction between the heavy photon and the Standard Model through the vector portal could be the leading interaction between the Standard Model and the Dark Sector (where the Dark Sector comprises the dark energy and dark matter which we can only observe indirectly through gravitational effects).

2.2.1 MEDIATOR OF DARK MATTER INTERACTIONS

Astrophysical observations of the rotational velocity of spiral galaxies has indicated the large presence of an unidentifiable mass contribution [4]. The simplest model to explain this additional mass contribution, Lambda Cold Dark Matter (ΛCDM), estimates that nearly one-third of the universe is composed of this dark matter while SM particles only compose some 4% of the universe. ΛCDM is consistent with measurements of the Cosmic Microwave Background (CMB) power spectrum which indicates the relative quantities of dark matter and SM matter [5]. The theory of ΛCDM requires no force beyond that of gravity for dark matter particles ("collisionless" dark matter), but discrepancies between simulation and observations indicate that the theory is still incomplete [6]. In particular, collisionless dark matter simulations generate cuspy dark matter halos with a changing density and velocity profile as well as halos containing significant structure. However, astrophysical observations indicate that the cores are of constant density and only a handful of subhalos have been observed in the Milky Way.

Weakly Interacting Massive Particles (WIMPs) have been a prime dark matter candidate for several decades with particles in the 10s of GeV to TeV mass range and interaction strengths characterized by the weak scale. While many experiments have been devoted to the detection of WIMPs through nuclear recoils and missing energy measurements, no confident signal has been detected [7]. Light dark matter with masses in the MeV to GeV range are strongly motivated as a theory that has been previously overlooked but could explain various astrophysical phenomena. In order to have the correct relic abundance in a theory of light dark matter, a new force is required to mediate dark matter interactions. The presence of a new boson force carrier can suppress the dark matter annihilation cross sections through a Somerfeld enhancement [8] and can only happen if the gauge boson has a mass of GeV scale and smaller. The Somerfeld enhancement boosts the annihilation cross section at lower velocities and yields the correct thermal relic abundance.

2.2.2 OBSERVATIONS FOR LIGHT DARK MATTER

An eXciting Dark Matter (XDM) model proposes that dark matter can scatter via a heavy photon into excited states that can subsequently decay into dark matter and a SM photon [9]. This process is shown in Figure 2.2.1.

This model could account for the observed 3.5 keV X-ray emission line observed in 73 galaxy clusters [10]. The cores of galaxies are of interest to study and look for signals of dark matter interactions. Additionally, observations of a gamma ray excess around the Galactic

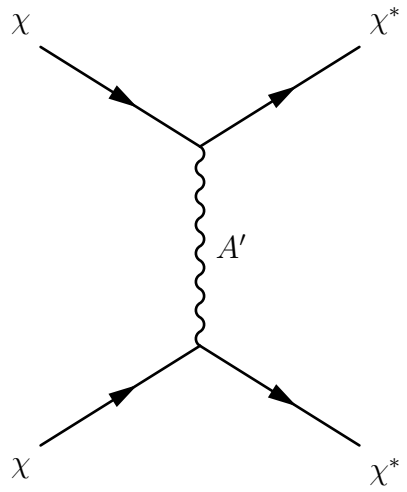

FIG. 2.2.1: The heavy photon mediates dark matter scattering into an excited state. Excited dark matter could subsequently decay producing observable X-ray emission spectra $\chi^* \to \chi\gamma$.

Center cannot be explained through known processes of interactions with cosmic rays and gamma rays from known sources [11]. This observation can be further explained through a model involving light dark matter interactions.

2.2.3 HISTORICAL MOTIVATORS

Astrophysical anomalies and tests of the SM have been historical motivators to explore a theory of light dark matter with a dark force mediator.

An excess in the positron fraction measured in cosmic rays was detected above 10 GeV by several different balloon payload experiments including HEAT [12] and CAPRICE [13] and confirmed in space telescopes such as PAMELA [14], the Fermi Large Area Telescope [15], and the Alpha Magnetic Spectrometer [16]. Positrons are known to be produced in interactions between cosmic ray nuclei and interstellar matter, but the excess was unforeseen from these sources alone. Alternatively, the measured anti-proton spectrum did not show an excess in the spectrum and was consistent with these secondary processes. These phenomena motivated a theory of light dark matter scattering mediated by a heavy photon with a mass $< 2m_p$ that could decay to lepton pairs. Further measurements of the positron spectrum from the AMS-02 should have yielded a bump in the positron excess at higher energies if the lepton pairs were the result of a heavy photon decay. As no apparent bump in this spectrum was observed [17], the data from AMS-02 is used to constrain theories of light dark matter [7].

The muon anomalous magnetic moment, $g-2$, was measured as having a larger than three standard deviation discrepancy than what is predicted by the SM [18]. This difference could be accounted for if there is an additional contribution from a heavy photon correction. Several experiments ruled out the possibility of a heavy photon that decays visibly being able to account for this effect, but a heavy photon that decays invisibly is still possibly responsible for this effect. The contribution from a heavy photon interaction to the muon $g-2$ is shown in Figure 2.2.2.

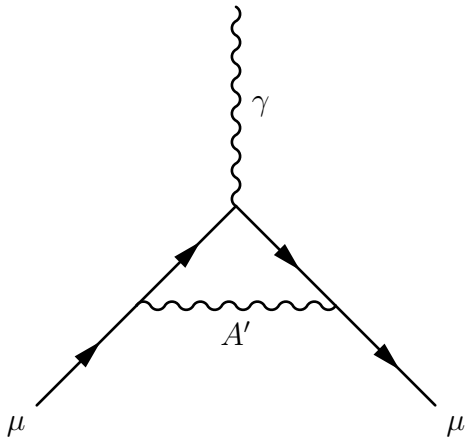

FIG. 2.2.2: Heavy photon contribution to the muon $g-2$.

2.3 SEARCHING FOR HEAVY PHOTONS

Due to the mechanism of kinetic mixing, the production of the heavy photon is similar to that of a photon radiating from an electron although at a suppressed rate proportional to the coupling ϵ^2. The final states into which the heavy photon can decay is related to the model of the dark sector and corresponding dark matter mass m_χ. A heavy photon that is heavier than $2m_\chi$ can decay into completely invisible states or a mixture of invisible states and SM states. Here, we focus solely on the scenario of a heavy photon that decays visibly to SM particles (this also implies that the heavy photon is lighter than twice the lightest dark matter mass).

2.3.1 DECAY SIGNATURE

The branching ratio of the heavy photon is obtained from the ratios of different final state measurements of $e^+e^- \rightarrow$ hadrons at various center-of-mass energies [7]. In the mass regime that HPS explores, the heavy photon will decay to e^+e^- pairs as shown in Figure 2.3.1.

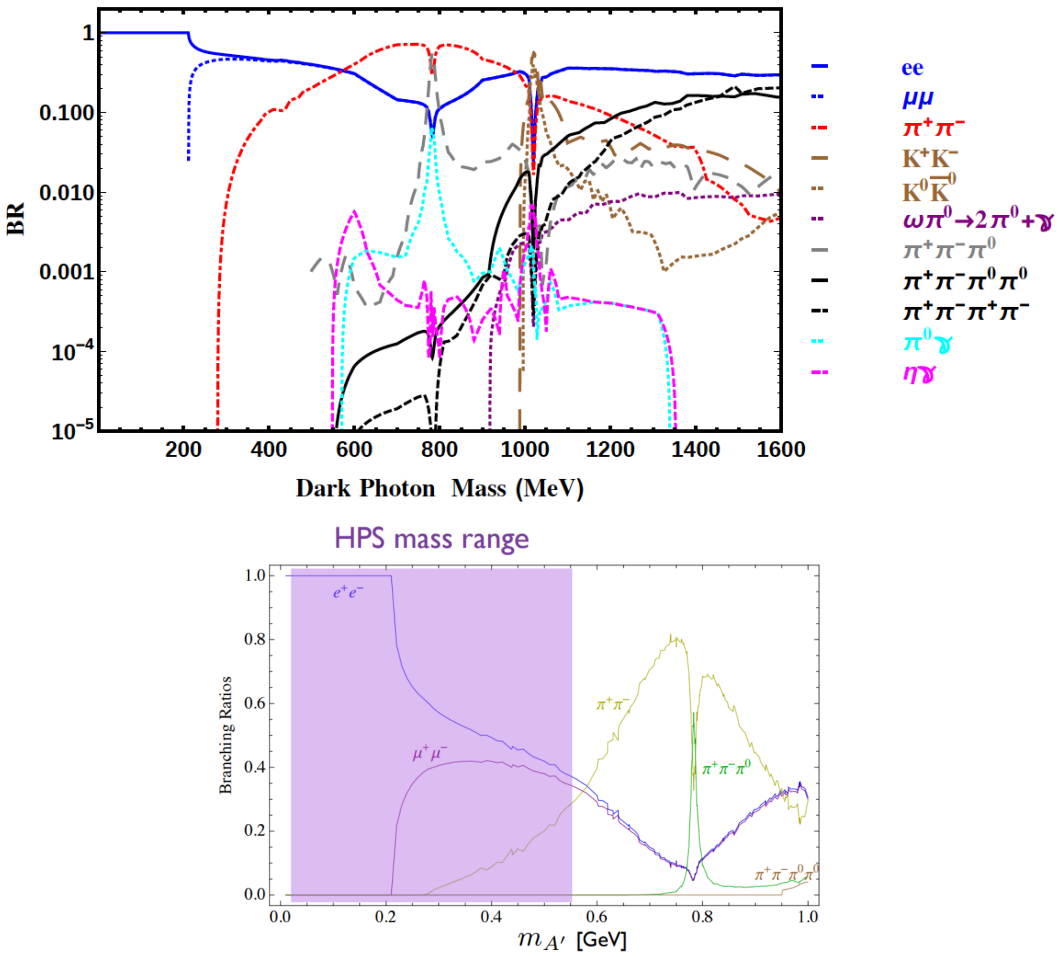

FIG. 2.3.1: The branching fraction ratios for heavy photons of various masses is shown [7]. The top plot is shown for an extended mass range and log scale whereas the bottom plot shows a more limited mass range and linear scaling. The mass range that HPS is most sensitive to is highlighted in purple in the bottom plot.

HPS searches for heavy photons of masses 20 to 100 MeV/c^2. As shown in Figure 2.3.1, at heavy photon masses above 200 MeV/c^2, the branching ratio for decays to e^+e^- decreases sharply and decays to $\mu^+\mu^-$ becomes significant.

Assuming that the heavy photon only decays to SM final states, the proper lifetime of the A' neglecting phase space corrections is described by

$$
\begin{aligned}
c\tau &= \frac{1}{\Gamma} \simeq \frac{3}{N_{eff} m_{A'} \alpha \epsilon^2} \\
&\simeq \frac{0.8 \text{ cm}}{N_{eff}} \Big(\frac{10^{-4}}{\epsilon}\Big)^2 \Big(\frac{100 \text{ MeV}}{m_{A'}}\Big)
\end{aligned}
\tag{2}
$$

where N_{eff} is the number of available decay states ($= 1$ at $m_{A'} < 2m_{\mu}$) [3]. The lifetime is inversely proportional to the coupling ϵ^2. For small couplings, the heavy photon will travel a measurable distance before decaying. The decay length is

$$
\begin{aligned}
l_0 &\equiv \gamma c\tau \\
&\simeq \frac{0.8 \text{ cm}}{N_{eff}} \Big(\frac{E_{beam}}{10 \text{ GeV}}\Big) \Big(\frac{10^{-4}}{\epsilon}\Big)^2 \Big(\frac{100 \text{ MeV}}{m_{A'}}\Big)^2
\end{aligned}
\tag{3}
$$

where E_{beam} is the incident electron energy. The rate of A' production is dependent on $\alpha^3 \epsilon^2 / m_{A'}^2$ and is suppressed relative to ordinary bremsstrahlung by a factor of $\epsilon^2 m_{e^-}^2 / m_{A'}^2$ [3]. The ratio of the fully differential production cross sections for the heavy photon relative to the production of a virtual photon is:

$$
\frac{d\sigma(e^- Z \to e^- Z A' \to e^- Z l^+ l^-)}{d\sigma(e^- Z \to e^- Z \gamma^* \to e^- Z l^+ l^-)} = \Big(\frac{3\pi\epsilon^2}{2N_{eff}\alpha}\Big)\Big(\frac{m_{A'}}{\delta m_{A'}}\Big) \tag{4}
$$

This ratio represents the maximum signal to background that can be achieved in an experiment. The heavy photon is produced at very forward, small angles and carries nearly all of the beam energy.

2.3.2 METHODS OF PRODUCTION

Heavy photons can be produced experimentally in fixed-target experiments and collider experiments. Fixed-target experiments are complementary to collider experiments in that they can generally access smaller coupling due to the high luminosity while collider experiments can probe higher heavy photon masses due to the higher center of mass energy attainable. In electron fixed-target experiments, the heavy photon is generated through a bremsstrahlung-like process and is detected from the final state particles. Proton fixed-target experiments look for the signal in the decay products of various mesons produced from the beam interaction with the target. Looking for heavy photons produced in meson decays such as Dalitz decays ($\pi^0, \eta, \eta' \to \gamma A'$), ($K \to \pi A'$, $\phi \to \eta A'$, and $D^* \to D^0 A'$) are another production mechanism that has been used at both colliders and fixed target-type experiments.

Drell-Yan ($q\bar{q} \to A'$) experiments are more common at proton fixed target and hadron collider experiments. Both e^+e^- colliders and hadron colliders search for heavy photons in the decay channels shown in Figure 2.3.1 and are particularly well-suited to search for heavy photons that decay invisibly due to their ability to precisely reconstruct the initial state.

2.3.3 METHODS OF DETECTION

The strategies for searching for heavy photons are typically a bump hunt on the visible final state particles, a bump hunt in the missing mass spectrum (for invisible decays), or a detached vertex search for heavy photons with small couplings.

Electron fixed-target experiments produce heavy photons through bremsstrahlung-like processes with the electron beam incident on a heavy target. Heavy photons are produced in a very forward direction requiring high resolution spectrometers or detectors close to the beam. Previous limits set by this type of experiment include the A1 experiment that uses the Microtron beam at Mainz and the A1 high resolution spectrometer to reconstruct the e^+e^- pair [19]. The A1 experiment significantly ruled out parameter space where the heavy photon was a possible explanation to resolve the muon $g-2$ anomaly. The APEX experiment at Jefferson Lab Hall A produced electron bremsstrahlung and used the high resolution spectrometers to measure the e^+e^- particles [20]. APEX performed a bump hunt on the final state particles in the mass range 65-600 MeV and will likely take data again in 2018. DarkLight is another Jefferson Lab experiment that places a windowless gas target in the Low Energy Recirculator Facility using a 100 MeV beam to search for heavy photons with low masses. DarkLight will perform a bump hunt search in the e^+e^- mass spectrum and may have some ability to search for invisible decays by using a silicon layer to detect proton recoils [21].

Proton fixed target experiments look for heavy photons in the decays of particles produced from beam interactions at the target. The NA48/2 experiment at the CERN SPS produced $K^{\pm}$ beams and searched for heavy photons from the π^0 decay produced from the in-flight decay of the $K^{\pm}$ [22]. SHiP is a future experiment at the CERN SPS that will use a 400 GeV proton beam to look in both Drell Yan and meson decays for heavy photons. SHiP will be sensitive to long decay lengths (on the order of 10s of meters) and will cover a wide mass range in visible decay states up to 10 GeV masses. SHiP is expected to run sometime after 2026 [23].

Beam dump experiments look for heavy photons with long decay lengths. The beam dump experiments E141 and E137 at SLAC, E774 at Fermilab, and one at Orsay were

originally run to look for MeV-mass axion-type particles from electron beam dumps [2]. The U70 beam dump looked for heavy photons downstream from a proton beam on a fixed target [24]. SeaQuest at Fermilab looks for muon pairs produced downstream from the 120 GeV proton beam on a fixed target. It is speculated that by analyzing previous data taken (E906/SeaQuest), a 95% confidence limit on heavy photon masses in the range of 215-5600 MeV is possible. SeaQuest is currently establishing upgrades for improved future running [25].

Collider experiments using e^+e^- or pp collisions complement the fixed-target experiments and are favored for looking for heavy photon invisible decays. BaBar, an experiment at the Stanford Linear Accelerator (SLAC) e^+e^- collider, set limits by searching for the A' in missing mass around the $\Upsilon(2S)$, $\Upsilon(3S)$, and $\Upsilon(4S)$ resonances [26]. In the near future, LHCb at CERN is expected to look for heavy photons in the di-muon invariant mass spectrum from rare heavy quark decays produced from proton-proton collisions. LHCb will be sensitive to the heavy photons with both prompt and displaced vertices and is expected to run sometime after 2021 [27]. The limits established by existing searches can be seen in Figure 1.0.1.

2.4 HEAVY PHOTON SEARCH KINEMATICS

The HPS experiment sends an electron beam through a thin tungsten target and looks for radiated heavy photons in the reconstructed e^+e^- mass spectrum. HPS looks for heavy photons in the range of 20 to 1000 MeV/c^2 and covers this territory with two searches on the same data set that probe different heavy photon coupling regimes. A bump hunt searches for the heavy photon signal as a resonance on a large background. The bump hunt looks for heavy photons with large couplings and decay at the target. The vertex search looks for heavy photons that have detached vertices, having a measurable lifetime and decaying downstream of the target.

2.4.1 SIGNAL

The heavy photon is generated from the electron beam interaction with a heavy target as shown in Figure 2.4.1 where Z is the atomic number corresponding to the target material.

Shown for the HPS experiment, the heavy photon decays to e^+e^- pairs with a measurable mass and possible displaced vertex downstream from the target. The differential cross section for heavy photon production is

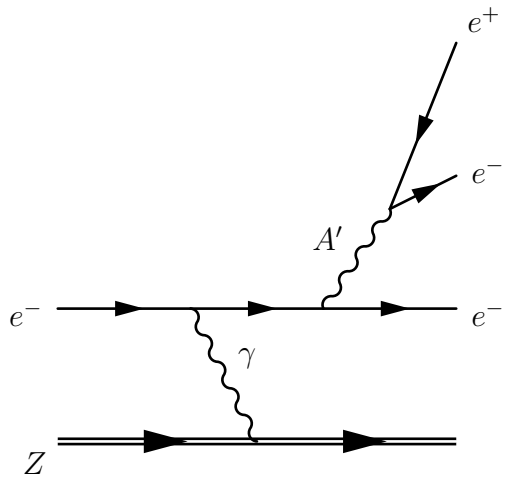

FIG. 2.4.1: The heavy photon is produced in a process analagous to bremsstrahlung on a heavy target of atomic number Z.

$$\frac{d\sigma}{dx d\cos\theta_{A'}} \approx \frac{8Z^2\alpha^3\epsilon^2 E_0^2 x}{U(x,\theta_{A'})^2}\log\Big((1-x+\frac{x^2}{2}) - \frac{x(1-x)m_{A'}^2 E_0^2 x\theta_{A'}^2}{U(x,\theta_{A'})^2}\Big) \tag{5}$$

where Z is the atomic number of the target material, α is the usual fine structure constant, $\theta_{A'}$ is the lab frame angle of the outgoing heavy photon, E_0 is the electron incident energy, $m_{A'}$ is the heavy photon mass, and the fraction of incident beam energy carried by the the heavy photon is $x \equiv E_{A'}/E_0$ [3]. The virtuality of the intermediate electron is described by

$$U(x,\theta_{A'}) = E_0^2 x\theta_{A'}^2 + m_{A'}^2\frac{1-x}{x} + m_e^2 x \tag{6}$$

where m_e is the mass of the electron. The cross section is further simplified for $m_e \ll m_{A'} \ll E_0$ and $x\theta_{A'}^2 \ll 1$. Integrating Equation (5) over the angle, the cross section is

$$\frac{d\sigma}{dx} \approx \frac{8Z^2\alpha^3\epsilon^2 x}{m_{A'}^2}\Big(1+\frac{x^2}{3(1-x)}\Big) \tag{7}$$

The total heavy photon production rate is proportional to $\alpha^3\epsilon^2/m_{A'}^2$ and is suppressed relative to photon bremsstrahlung by $\epsilon^2 m_e^2/m_{A'}^2$.The singularity is regulated by the mass of the electron and cutoff for values where $1-x$ exceeds $m_e^2/m_{A'}^2$ or $m_{A'}^2/E_0^2$. The heavy photon carries nearly the entire beam energy such that the median value of $1-x \sim \max\Big(\frac{m_e}{m_{A'}}, \frac{m_{A'}}{E_0}\Big)$. The heavy photon is emitted predominately at small angles with a cutoff at $\frac{m_{A'}^{3/2}}{E_0^{3/2}}$ such that the angular emission falls off as $1/\theta_{A'}^4$.

The heavy photon is characterized by its mass (as reconstructed from the decay to e^+e^-)

and decay length. Depending on the coupling strength ϵ, the vertex may be reconstructed from a prompt decay at the target or a measurable decay downstream.

2.4.2 BACKGROUNDS

The primary backgrounds in this experiment include trident events and wide angle bremsstrahlung (WAB). The tridents have the same three particle final state $e^-e^-e^+$ and are broadly categorized into radiative and Bethe-Heitler diagrams [3]. The trident events were the primary source of background considered prior to running the experiment. It was later found that WAB events contributed to the background with an $e^-\gamma$ final state where the photon then produced an e^+e^-. In many cases, the event was triggered by the initial electron and pair-produced positron.

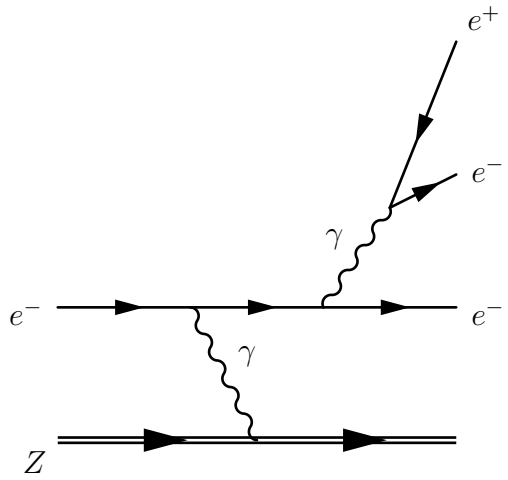

FIG. 2.4.2: Radiative trident background process: The photon is radiated from the electron incident on a heavy target of atomic number Z and produces and e^+e^- pair. The radiatives have the same kinematics as the heavy photon and comprise the primary background in the bump hunt analysis where all decays are prompt.

The radiative background is irreducible and comprises the smooth background upon which the bump hunt search for the heavy photon signal is conducted. The Bethe-Heitler tridents also contribute significantly to the background although they are peaked at lower e^+e^- total energy. The Bethe-Heitler contribution is shown in Figure 2.4.3. The radiative and Bethe-Heitler diagrams also interfere, although, this generally only contributes at lower e^+e^- total energy.

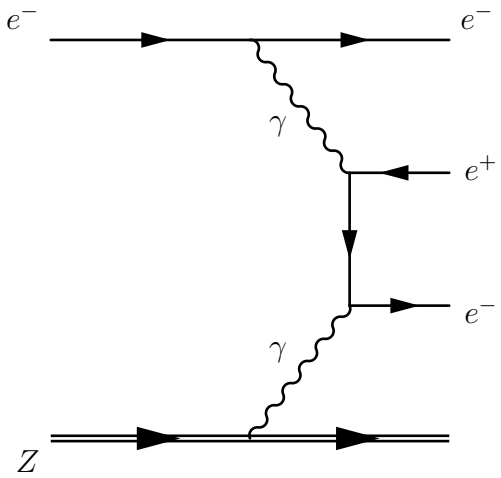

FIG. 2.4.3: Bethe-Heitler trident background process: The photon produced from electron interaction at a target of atomic number Z produces an e^+e^- pair that often have a total energy much less than the initial beam energy. The recoil electron and the Bethe-Heitler positron can also be detected.

CHAPTER 3

HEAVY PHOTON SEARCH EXPERIMENT

CHAPTER 4

DETECTOR CALIBRATION AND PERFORMANCE

CHAPTER 5

SEARCHING FOR DISPLACED VERTICES

CHAPTER 6

VERTEX SEARCH RESULTS

CHAPTER 7

CONCLUSION

The Heavy Photon Search experiment successfully took data during the spring 2015 and 2016 engineering runs. The detectors and beam performed well and consistently with that which was proposed and simulated. This thesis presents details of the simulation and calibration of the ECal and its performance in both runs. The first results of the unblinded, full 2015 vertex analysis using data from multiple SVT layer combinations and different SVT settings is presented.

It has been shown that the proposal vertex anticipated exclusion made assumptions about the detector acceptance that are not consistent with Monte Carlo and experimental data. No exclusion is obtained from the 2015 run, but the procedure for searching for displaced vertices and the acceptance-related effects have been fully developed and presented here. The procedure for combining the data sets from different SVT layer combinations has been discussed. L1L2 and L2L2 contributions in the 0.5 mm data have too much background to have a $zCut$ low enough for these data to contribute to the overall reach. The L1L2 and L2L2 contributions in the 1.5 mm data have less excess high z backgrounds, but the statistics of the data is too low to contribute to the reach. Additionally, there are excess background events that contaminate the vertex analysis and will require further study after the improved implementation of the vertex reconstruction code in the near future.

HPS has a promising future with more beam time scheduled and planned upgrades that will improve the vertex reach. The addition of a hodoscope in front of the positron side of the ECal will improve the trigger by eliminating triggers from photons from Wide Angle Bremsstrahlung and recovering events where the electron are lost in the ECal hole. A Layer 0 at 5 cm downstream of the target will improve the vertex resolution of the SVT by enabling tighter $zCut$s. The excess backgrounds will continue to be studied from both runs.

BIBLIOGRAPHY

[1] Bob Holdom. Two U(1)'s and charge shifts. 166(2):196–198.

[2] Jim Alexander, Marco Battaglieri, Bertrand Echenard, Rouven Essig, Matthew Graham, Eder Izaguirre, John Jaros, Gordan Krnjaic, Jeremy Mardon, David Morrissey, Tim Nelson, Maxim Perelstein, Matt Pyle, Adam Ritz, Philip Schuster, Brian Shuve, Natalia Toro, Richard G. Van De Water, Daniel Akerib, Haipeng An, Konrad Aniol, Isaac J. Arnquist, David M. Asner, Henning O. Back, Keith Baker, Nathan Baltzell, Dipanwita Banerjee, Brian Batell, Daniel Bauer, James Beacham, Jay Benesch, James Bjorken, Nikita Blinov, Celine Boehm, Mariangela Bond, Walter Bonivento, Fabio Bossi, Stanley J. Brodsky, Ran Budnik, Stephen Bueltmann, Masroor H. Bukhari, Raymond Bunker, Massimo Carpinelli, Concetta Cartaro, David Cassel, Gianluca Cavoto, Andrea Celentano, Animesh Chaterjee, Saptarshi Chaudhuri, Gabriele Chiodini, Hsiao-Mei Sherry Cho, Eric D. Church, D. A. Cooke, Jodi Cooley, Robert Cooper, Ross Corliss, Paolo Crivelli, Francesca Curciarello, Annalisa D'Angelo, Hooman Davoudiasl, Marzio De Napoli, Raffaella De Vita, Achim Denig, Patrick deNiverville, Abhay Deshpande, Ranjan Dharmapalan, Bogdan Dobrescu, Sergey Donskov, Raphael Dupre, Juan Estrada, Stuart Fegan, Torben Ferber, Clive Field, Enectali Figueroa-Feliciano, Alessandra Filippi, Bartosz Fornal, Arne Freyberger, Alexander Friedland, Iftach Galon, Susan Gardner, Francois-Xavier Girod, Sergei Gninenko, Andrey Golutvin, Stefania Gori, Christoph Grab, Enrico Graziani, Keith Griffioen, Andrew Haas, Keisuke Harigaya, Christopher Hearty, Scott Hertel, JoAnne Hewett, Andrew Hime, David Hitlin, Yonit Hochberg, Roy J. Holt, Maurik Holtrop, Eric W. Hoppe, Todd W. Hossbach, Lauren Hsu, Phil Ilten, Joe Incandela, Gianluca Inguglia, Kent Irwin, Igal Jaegle, Robert P. Johnson, Yonatan Kahn, Grzegorz Kalicy, Zhong-Bo Kang, Vardan Khachatryan, Venelin Kozhuharov, N. V. Krasnikov, Valery Kubarovsky, Eric Kuflik, Noah Kurinsky, Ranjan Laha, Gaia Lanfranchi, Dale Li, Tongyan Lin, Mariangela Lisanti, Kun Liu, Ming Liu, Ben Loer, Dinesh Loomba, Valery E. Lyubovitskij, Aaron Manalaysay, Giuseppe Mandaglio, Jeremiah Mans, W. J. Marciano, Thomas Markiewicz, Luca Marsicano, Takashi Maruyama, Victor A. Matveev, David McKeen, Bryan McKinnon, Dan McKinsey, Harald Merkel, Jeremy Mock, Maria Elena Monzani, Omar Moreno, Corina Nantais, Sebouh Paul, Michael Peskin, Vladimir Poliakov, Antonio D. Polosa, Maxim Pospelov, Igor Rachek, Balint Radics, Mauro Raggi, Nunzio Randazzo,

Blair Ratcliff, Alessandro Rizzo, Thomas Rizzo, Alan Robinson, Andre Rubbia, David Rubin, Dylan Rueter, Tarek Saab, Elena Santopinto, Richard Schnee, Jessie Shelton, Gabriele Simi, Ani Simonyan, Valeria Sipala, Oren Slone, Elton Smith, Daniel Snowden-Ifft, Matthew Solt, Peter Sorensen, Yotam Soreq, Stefania Spagnolo, James Spencer, Stepan Stepanyan, Jan Strube, Michael Sullivan, Arun S. Tadepalli, Tim Tait, Mauro Taiuti, Philip Tanedo, Rex Tayloe, Jesse Thaler, Nhan V. Tran, Sean Tulin, Christopher G. Tully, Sho Uemura, Maurizio Ungaro, Paolo Valente, Holly Vance, Jerry Vavra, Tomer Volansky, Belina von Krosigk, Andrew Whitbeck, Mike Williams, Peter Wittich, Bogdan Wojtsekhowski, Wei Xue, Jong Min Yoon, Hai-Bo Yu, Jaehoon Yu, Tien-Tien Yu, Yue Zhang, Yue Zhao, Yiming Zhong, and Kathryn Zurek. Dark Sectors 2016 Workshop: Community Report.

[3] James D. Bjorken, Rouven Essig, Philip Schuster, and Natalia Toro. New Fixed-Target Experiments to Search for Dark Gauge Forces. 80(7).

[4] Yoshiaki Sofue and Vera Rubin. Rotation curves of spiral galaxies. *Ann. Rev. Astron. Astrophys.*, 39:137–174, 2001.

[5] Mathew S. Madhavacheril, Neelima Sehgal, and Tracy R. Slatyer. Current Dark Matter Annihilation Constraints from CMB and Low-Redshift Data. 89(10).

[6] David H. Weinberg, James S. Bullock, Fabio Governato, Rachel Kuzio de Naray, and Annika H. G. Peter. Cold dark matter: Controversies on small scales.

[7] Jia Liu, Neal Weiner, and Wei Xue. Signals of a Light Dark Force in the Galactic Center. 2015(8).

[8] Nima Arkani-Hamed, Douglas P. Finkbeiner, Tracy R. Slatyer, and Neal Weiner. A Theory of Dark Matter. 79(1).

[9] Douglas P. Finkbeiner and Neal Weiner. An X-Ray Line from eXciting Dark Matter.

[10] Esra Bulbul, Maxim Markevitch, Adam Foster, Randall K. Smith, Michael Loewenstein, and Scott W. Randall. Detection of An Unidentified Emission Line in the Stacked X-ray spectrum of Galaxy Clusters. 789(1):13.

[11] Dan Hooper and Lisa Goodenough. Dark Matter Annihilation in The Galactic Center As Seen by the Fermi Gamma Ray Space Telescope. *Phys. Lett.*, B697:412–428, 2011.

[12] S. W. Barwick et al. Cosmic ray positrons at high-energies: A New measurement. *Phys. Rev. Lett.*, 75:390–393, 1995.

[13] M. Boezio et al. Measurements of cosmic-ray electrons and positrons by the Wizard/CAPRICE collaboration. *Adv. Space Res.*, 27(4):669–674, 2001.

[14] O. Adriani, G. C. Barbarino, G. A. Bazilevskaya, R. Bellotti, M. Boezio, E. A. Bogomolov, L. Bonechi, M. Bongi, V. Bonvicini, S. Bottai, A. Bruno, F. Cafagna, D. Campana, P. Carlson, M. Casolino, G. Castellini, M. P. De Pascale, G. De Rosa, N. De Simone, V. Di Felice, A. M. Galper, L. Grishantseva, P. Hofverberg, S. V. Koldashov, S. Y. Krutkov, A. N. Kvashnin, A. Leonov, V. Malvezzi, L. Marcelli, W. Menn, V. V. Mikhailov, E. Mocchiutti, S. Orsi, G. Osteria, P. Papini, M. Pearce, P. Picozza, M. Ricci, S. B. Ricciarini, M. Simon, R. Sparvoli, P. Spillantini, Y. I. Stozhkov, A. Vacchi, E. Vannuccini, G. Vasilyev, S. A. Voronov, Y. T. Yurkin, G. Zampa, N. Zampa, and V. G. Zverev. Observation of an anomalous positron abundance in the cosmic radiation. 458(7238):607–609.

[15] S. Abdollahi et al. Cosmic-ray electron-positron spectrum from 7 GeV to 2 TeV with the Fermi Large Area Telescope. *Phys. Rev.*, D95(8):082007, 2017.

[16] Stefan Schael. Cosmic positron spectrum measurement from 1 to 50 GeV with AMS-01. In *Proceedings, 30th International Cosmic Ray Conference (ICRC 2007): Merida, Yucatan, Mexico, July 3-11, 2007*, volume 4, pages 753–756, 2007.

[17] Lars Bergstrom, Torsten Bringmann, Ilias Cholis, Dan Hooper, and Christoph Weniger. New limits on dark matter annihilation from AMS cosmic ray positron data. *Phys. Rev. Lett.*, 111:171101, 2013.

[18] Thomas Blum, Achim Denig, Ivan Logashenko, Eduardo de Rafael, B. Lee Roberts, Thomas Teubner, and Graziano Venanzoni. The Muon (g-2) Theory Value: Present and Future.

[19] T. Beranek, H. Merkel, and M. Vanderhaeghen. Theoretical framework to analyze searches for hidden light gauge bosons in electron scattering fixed target experiments. 88(1):015032.

[20] S. Abrahamyan, Z. Ahmed, K. Allada, D. Anez, T. Averett, A. Barbieri, K. Bartlett, J. Beacham, J. Bono, J. R. Boyce, P. Brindza, A. Camsonne, K. Cranmer, M. M.

Dalton, C. W. deJager, J. Donaghy, R. Essig, C. Field, E. Folts, A. Gasparian, N. Goeckner-Wald, J. Gomez, M. Graham, J.-O. Hansen, D. W. Higinbotham, T. Holmstrom, J. Huang, S. Iqbal, J. Jaros, E. Jensen, A. Kelleher, M. Khandaker, J. J. LeRose, R. Lindgren, N. Liyanage, E. Long, J. Mammei, P. Markowitz, T. Maruyama, V. Maxwell, S. Mayilyan, J. McDonald, R. Michaels, K. Moffeit, V. Nelyubin, A. Odian, M. Oriunno, R. Partridge, M. Paolone, E. Piasetzky, I. Pomerantz, Y. Qiang, S. Riordan, Y. Roblin, B. Sawatzky, P. Schuster, J. Segal, L. Selvy, A. Shahinyan, R. Subedi, V. Sulkosky, S. Stepanyan, N. Toro, D. Walz, B. Wojtsekhowski, and J. Zhang. Search for a new gauge boson in the A' Experiment (APEX). 107(19).

[21] J. Balewski, J. Bernauer, J. Bessuille, R. Corliss, R. Cowan, C. Epstein, P. Fisher, D. Hasell, E. Ihloff, Y. Kahn, J. Kelsey, R. Milner, S. Steadman, J. Thaler, C. Tschalaer, C. Vidal, S. Benson, J. Boyce, D. Douglas, P. Evtushenko, C. Hernandez-Garcia, C. Keith, C. Tennant, S. Zhang, R. Alarcon, D. Blyth, R. Dipert, L. Ice, G. Randall, B. Dongwi, N. Kalantarians, M. Kohl, A. Liyanage, J. Nazeer, M. Garcon, R. Cervantes, K. Dehmelt, A. Deshpande, N. Feege, and B. Surrow. The DarkLight Experiment: A Precision Search for New Physics at Low Energies.

[22] J. R. Batley et al. Search for the dark photon in π^0 decays. *Phys. Lett.*, B746:178–185, 2015.

[23] SHiP Collaboration, M. Anelli, S. Aoki, G. Arduini, J. J. Back, A. Bagulya, W. Baldini, A. Baranov, G. J. Barker, S. Barsuk, M. Battistin, J. Bauche, A. Bay, V. Bayliss, L. Bellagamba, G. Bencivenni, M. Bertani, O. Bezshyyko, D. Bick, N. Bingefors, A. Blondel, M. Bogomilov, A. Boyarsky, D. Bonacorsi, D. Bondarenko, W. Bonivento, J. Borburgh, T. Bradshaw, R. Brenner, D. Breton, N. Brook, M. Bruschi, A. Buonaura, S. Buontempo, S. Cadeddu, A. Calcaterra, M. Calviani, M. Campanelli, C. Capoccia, A. Cecchetti, A. Chatterjee, J. Chauveau, A. Chepurnov, M. Chernyavskiy, P. Ciambrone, C. Cicalo, G. Conti, K. Cornelis, M. Courthold, M. G. Dallavalle, N. D'Ambrosio, G. De Lellis, M. De Serio, L. Dedenko, A. Di Crescenzo, N. Di Marco, C. Dib, J. Dietrich, H. Dijkstra, D. Domenici, S. Donskov, D. Druzhkin, J. Ebert, U. Egede, A. Egorov, V. Egorychev, M. A. El Alaoui, T. Enik, A. Etenko, F. Fabbri, L. Fabbri, G. Fedorova, G. Felici, M. Ferro-Luzzi, R. A. Fini, M. Franke, M. Fraser, G. Galati, B. Giacobbe, B. Goddard, L. Golinka-Bezshyyko, D. Golubkov, A. Golutvin, D. Gorbunov, E. Graverini, J.-L. Grenard, A. M. Guler, C. Hagner, H. Hakobyan, J. C. Helo, E. van

Herwijnen, D. Horvath, M. Iacovacci, G. Iaselli, R. Jacobsson, I. Kadenko, M. Kamiscioglu, C. Kamiscioglu, G. Khaustov, A. Khotjansev, B. Kilminster, V. Kim, N. Kitagawa, K. Kodama, A. Kolesnikov, D. Kolev, M. Komatsu, N. Konovalova, S. Koretskiy, I. Korolko, A. Korzenev, S. Kovalenko, Y. Kudenko, E. Kuznetsova, H. Lacker, A. Lai, G. Lanfranchi, A. Lauria, H. Lebbolo, J.-M. Levy, L. Lista, P. Loverre, A. Lukiashin, V. E. Lyubovitskij, A. Malinin, M. Manfredi, A. Perillo-Marcone, A. Marrone, R. Matev, E. N. Messomo, P. Mermod, S. Mikado, Yu Mikhaylov, J. Miller, D. Milstead, O. Mineev, R. Mingazheva, G. Mitselmakher, M. Miyanishi, P. Monacelli, A. Montanari, M. C. Montesi, G. Morello, K. Morishima, S. Movtchan, V. Murzin, N. Naganawa, T. Naka, M. Nakamura, T. Nakano, N. Nurakhov, B. Obinyakov, K. Ocalan, S. Ogawa, V. Oreshkin, A. Orlov, J. Osborne, P. Pacholek, J. Panman, A. Paoloni, L. Paparella, A. Pastore, M. Patel, K. Petridis, M. Petrushin, M. Poli-Lener, N. Polukhina, V. Polyakov, M. Prokudin, G. Puddu, F. Pupilli, F. Rademakers, A. Rakai, T. Rawlings, F. Redi, S. Ricciardi, R. Rinaldesi, T. Roganova, A. Rogozhnikov, H. Rokujo, A. Romaniouk, G. Rosa, I. Rostovtseva, T. Rovelli, O. Ruchayskiy, T. Ruf, G. Saitta, V. Samoylenko, V. Samsonov, A. Sanz Ull, A. Saputi, O. Sato, W. Schmidt-Parzefall, N. Serra, S. Sgobba, M. Shaposhnikov, P. Shatalov, A. Shaykhiev, L. Shchutska, V. Shevchenko, H. Shibuya, Y. Shitov, S. Silverstein, S. Simone, M. Skorokhvatov, S. Smirnov, E. Solodko, V. Sosnovtsev, R. Spighi, M. Spinetti, N. Starkov, B. Storaci, C. Strabel, P. Strolin, S. Takahashi, P. Teterin, V. Tioukov, D. Tommasini, D. Treille, R. Tsenov, T. Tshchedrina, A. Ustyuzhanin, F. Vannucci, V. Venturi, M. Villa, Heinz Vincke, Helmut Vincke, M. Vladymyrov, S. Xella, M. Yalvac, N. Yershov, D. Yilmaz, A. U. Yilmazer, G. Vankova-Kirilova, Y. Zaitsev, and A. Zoccoli. A facility to Search for Hidden Particles (SHiP) at the CERN SPS.

[24] Johannes Blmlein and Jrgen Brunner. New Exclusion Limits on Dark Gauge Forces from Proton Bremsstrahlung in Beam-Dump Data. *Phys. Lett.*, B731:320–326, 2014.

[25] S. Gardner, R. J. Holt, and A. S. Tadepalli. New Prospects in Fixed Target Searches for Dark Forces with the SeaQuest Experiment at Fermilab. 93(11).

[26] J. P. Lees et al. Search for a Dark Photon in e^+e^- Collisions at BaBar. *Phys. Rev. Lett.*, 113(20):201801, 2014.

[27] Philip Ilten, Yotam Soreq, Jesse Thaler, Mike Williams, and Wei Xue. Proposed Inclusive Dark Photon Search at LHCb. *Phys. Rev. Lett.*, 116(25):251803, 2016.

APPENDIX A

VERTEX RECONSTRUCTION EFFICIENCIES

The 0.5 mm reconstructed vertex efficiency, ϵ_{vtx} is described by the following parameterizations. For the L1L1 dataset fit by Equation (**??**), the parameters are shown in Equation 8.

$$\begin{aligned} p_0 &= -0.2359 + 3.606m \\ p_1 &= -0.03537 + 0.5395m \\ p_2 &= -0.001201 + 0.1404m - 2.614m^2 + 10.65m^3 \\ p_3 &= -0.0002078 + 0.008753m - 0.1396m^2 + 0.8077m^3 \end{aligned} \tag{8}$$

For the L1L2 dataset with the SVT at 0.5 mm from the beam, the parameters fit to Equation (**??**) are described by Equation (9).

$$\begin{aligned} z_{mean} &= -58.89 + 5208.95m - 76469.9m^2 + 386631m^3 \\ \sigma &= 3.05 + 629.99m - 14691.8m^2 + 114123m^3 \\ N &= -0.3125 + 37.0172m - 472.052m^2 \end{aligned} \tag{9}$$

For the L2L2 dataset with the SVT at 0.5 mm from the beam, the parameters fit to Equation (**??**) are described by Equation (10).

$$\begin{aligned} N &= -0.3623 + 30.88m - 374.7m^2 \\ z_{mean} &= -71.7603 + 7733.51m - 131569m^2 + 827080m^3 \\ \sigma &= -4.058 - 813m - 8947m^2 \end{aligned} \tag{10}$$

The 1.5 mm reconstructed vertex efficiency, ϵ_{vtx} is described by the following parameterizations. For the L1L1 dataset fit by Equation (**??**), the parameters are shown in Equation 11.

$$\begin{aligned} p_0 &= (m < 0.029) \times (194.3m - 5.9590) + (m \geq 0.029) \times (4.937m - 0.3635) \\ p_1 &= (m < 0.032) \times (19.52m - 0.6578) + (m \geq 0.032) \times (-9.889m^2 + 1.928m - 0.09032) \\ p_2 &= -0.01753 + 0.8977m - 13.89m^2 + 65.14m^3 \\ p_3 &= (m < 0.0285) \times (0.3299m - 0.009391) + (m \geq 0.0285) \times (0.001647m - 0.0001239) \end{aligned} \tag{11}$$

For the L1L2 dataset with the SVT at 1.5 mm from the beam, the parameters fit to Equation (**??**) are described by Equation (12).

$$\begin{aligned} z_{mean} &= -72.7326 + 4494.67m - 40308.4m^2 \\ \sigma &= 7.7148 + 79.5054m \\ N &= -0.3178 + 22.8208m - 253.373m^2 \end{aligned} \tag{12}$$

For the L2L2 dataset with the SVT at 1.5 mm from the beam, the parameters fit to Equation (**??**) are described by Equation (13).

$$\begin{aligned} N &= -0.3623 + 30.8816m - 374.691m^2 \\ z_{mean} &= -71.6658 + 7732.18m - 131207m^2 + 823016m^3 \\ \sigma &= -8.9366 + 1109.97m - 13284.4m^2 \end{aligned} \tag{13}$$

APPENDIX B

VERTEX ANALYSIS CUTS

B.0.1 L1L1 CUTS

The cut on the track quality χ^2 is shown in Figure B.0.1. Here, we cut on the individual positron and electron track qualities requiring a χ^2 to be less than 30.

The cut on the maximum electron track momentum is intended to reduce contamination from elastically-scattered electrons and to correspond to the range of electron energy expected from trident events. The cut is shown in Figure B.0.2.

A cut to the cluster time difference is set at ± 2 ns. This includes events from two beam buckets as shown in Figure B.0.3.

The difference between the unconstrained and beam spot constrained vertex χ^2 shows how well a vertexed e^+e^- pair's total momentum projects back to the beam spot position at the target. The cut is shown in Figure B.0.4.

The cut to SVT tracks matched to ECal clusters is shown in Figure B.0.5. The matching parameter was derived empirically from data and corresponds to the number σ, derived from the distribution difference of the projected track to the ECal and ECal cluster positions.

The momentum asymmetry cut is defined as the momentum difference over the momentum sum of the e^+e^- tracks. The momentum symmetry is intended to reduce the background WAB contamination. The effects of the cut are shown in Figure B.0.6.

The cut on the positron $DOCA$ is specifically intended to remove WAB contamination and downstream vertices from the pair-produced positron. The effects of the cut to the positron $DOCA$ on the vertex distribution are shown in Figure B.0.7.

Several downstream false vertices are produced that have a one hit difference with other tracks. Many of the tracks that share a lot of hits have nearly the same momentum as other tracks as shown in Figure B.0.8.

B.0.2 L1L2 WITH SVT AT 0.5 MM

The L1L2 data set with the SVT at the nominal 0.5 mm position consists of tracks where the one track missed the active region of Layer 1. This data set combines the case for which

the electron passes through Layer 1 and the positron passes through Layer 1 in order to obtaining the $zCut$ because it was noted that the tails of the distributions are the same (despite the known backgrounds being different and could merit improved cuts that would divide the data set in the future).

The cuts applied to the L1L2 data set are shown in Table 1.

The initial selection requires that a track that missed Layer 1 has a projection to the z location at layer 1 that is less than 1.5 mm from the beam. This ensures that the sample is not overly contaminated by events that passed through the active region but failed to identify a hit. As a result, the core of the distribution sits on the downstream side of the z-axis and reflects the geometric constraints we have imposed. The first cut that is different from the L1L1 data set is the isolation cut. In this data set, we apply the same isolation cut to the track that passed through Layer 1, but we apply a slightly different isolation cut for the track that did not pass through layer 1. The isolation in layer 2 is measured and projected to the target position to be compared with the impact parameter of the track in y at the target. Additional cuts are applied to the tails of the kink distributions for the tracks. The summary of these cuts is made in the Table 2.

The uncut kink distributions for the electron with the cut indicated by the red dashed line is shown in Figures B.0.9, B.0.10, and B.0.11.

The positron kink distributions look similar to the electron kink distributions and are not shown here. These cuts remove events from the tails. The effects of all the cuts on the reconstructed vertex position distribution are shown in Figure B.0.12.

The effects of the cuts on the reconstructed mass distribution are shown in Figure B.0.13.

This dataset has the tendency to contain more WAB contamination than the L1L1 data set. In particular, we know from Monte Carlo that positrons are unlikely to have a hit in Layer 1 when the photon in WAB pair produces after the target. Additionally, this sample contains a 5:1 ratio of having in electron versus a positron in the first layer.

B.0.3 L2L2 WITH SVT AT 0.5 MM

The L2L2 dataset consists of vertices produced when tracks do not pass through Layer 1 and their projections back to Layer 1 are within 1.5 mm of the beam (outside the active silicon region). This data set requires the most work to remove the background events, and preliminary studies with the small number of statistics have been unsuccessful.

The general cuts applied to the L2L2 data set, after first requiring that track projections do not extend to the active region of Layer 1, are listed in Table 3.

The geometric acceptance of the cuts in the L2L2 data set leave a core fraction of background events well beyond the target at approximately 30 mm downstream. The only modifications to previously applied cuts are that both tracks use a modified isolation cut by looking at the isolation at Layer 2 and the tracks do not share 4 hits with any other track in the event. The kink cuts appeared to not remove events from this data set.

B.0.4 L1L1 WITH SVT AT 1.5 MM

The L1L1 data set in the 1.5 mm data includes vertices reconstructed from pairs of tracks that have hits in Layer 1 of the SVT. Due to the SVT opening being larger, the acceptance favors larger heavy photon masses. The SVT has also lower rates in Layer 1 when compared to the 0.5 mm data set.

The cuts applied to the L1L1 data set are shown in Table 4.

The cuts are the same as those applied to the 0.5 mm data set with similar effect.

B.0.5 L1L2 WITH SVT AT 1.5 MM

The following section describes the data set where one track misses Layer 1 of the SVT and its track projection back to Layer 1 is within 2.5 mm of the beam such that the track does not extrapolate to the active region of the silicon.

The cuts applied to the L1L2 dataset with the first layer of the SVT at 1.5 mm is shown in Table 5.

The cuts applied to the L1L2 data set may require a similar optimization to eliminate backgrounds as that required of the data set for the 0.5 mm. Namely, that, it may be necessary to separate the data set for events where the positron versus the electron is the first to leave a hit in Layer 1. For the moment, the same cuts are used as the 1.5 mm data set has generally lower backgrounds than that seen in the 0.5 mm data set.

B.0.6 L2L2 WITH SVT AT 1.5 MM

The following section discusses the events having no hit in Layer 1 of the 1.5 mm data set. An additional requirement was made that the tracks must not project back to the active region of the Layer 1 silicon in order to avoid contamination by events with the Layer 1 inefficiency.

The cuts applied to the L2L2 data set are shown in Table 6.

The cuts are the same as those applied to the data in the 0.5 mm L2L2 data set. This

data set has significantly more statistics that needs to be studied and may complement the analysis on the 0.5 mm high z background data.

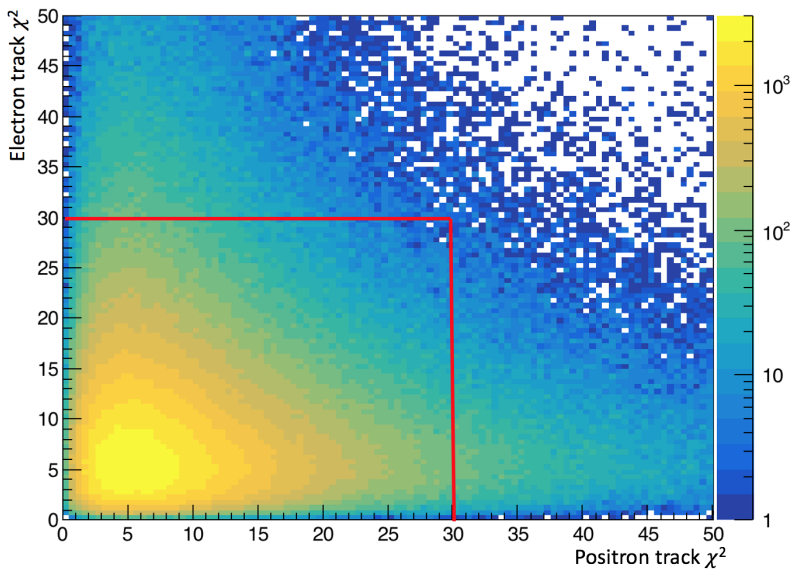

FIG. B.0.1: The electron and positron track χ^2 are shown with the cut indicated by the red line. This cut is an initial track selection quality cut and uses no vertex or timing information.

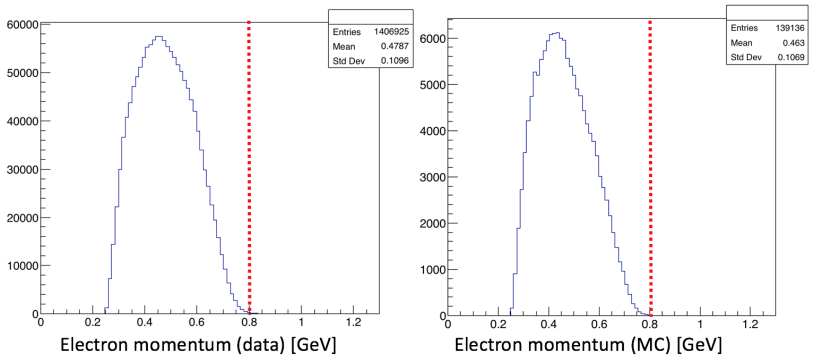

FIG. B.0.2: The maximum momentum of the electron track as shown in data (prior to cutting) and Monte Carlo. Events with higher electron energies are attributable to other types of backgrounds in the data such as elastics and wide angle bremsstrahlung and not the trident background.

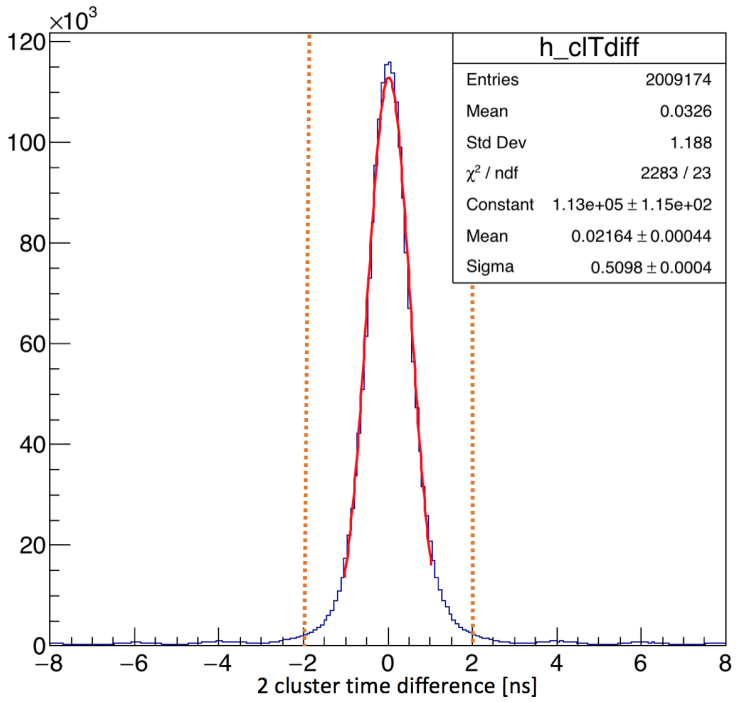

FIG. B.0.3: The two cluster timing difference is shown with a fit to the Gaussian central part of the distribution. Additional smaller peaks can be seen in intervals of 2 ns in the tails of the distribution. The timing cut can remove these events where the electron and positron come from different events.

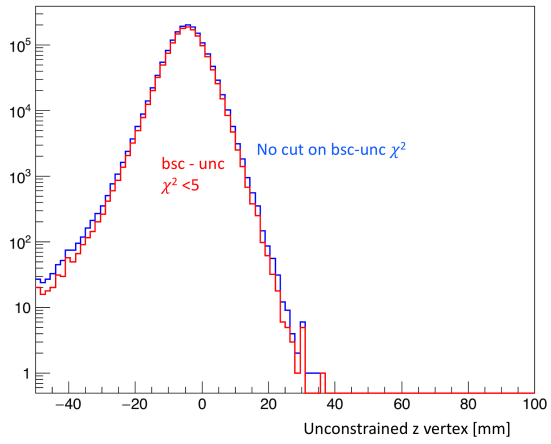

FIG. B.0.4: The effect of a cut on the difference between the beamspot and unconstrained constrained χ^2 on the vertex distribution for all masses. The effects of the cut on the downstream tails of the distribution tells us how well a vertexed pair of tracks points back to the beamspot position at the target.

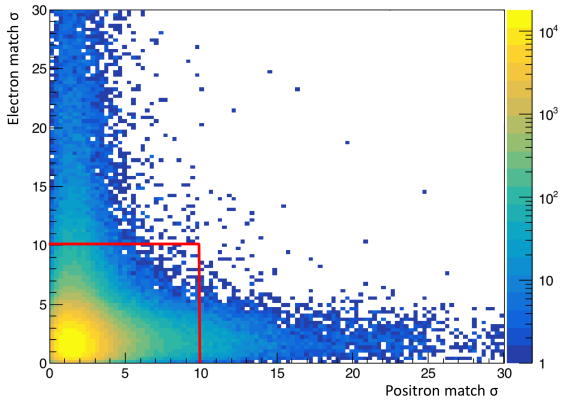

FIG. B.0.5: The SVT track to ECal cluster matching parameter for both electrons and positrons is shown.

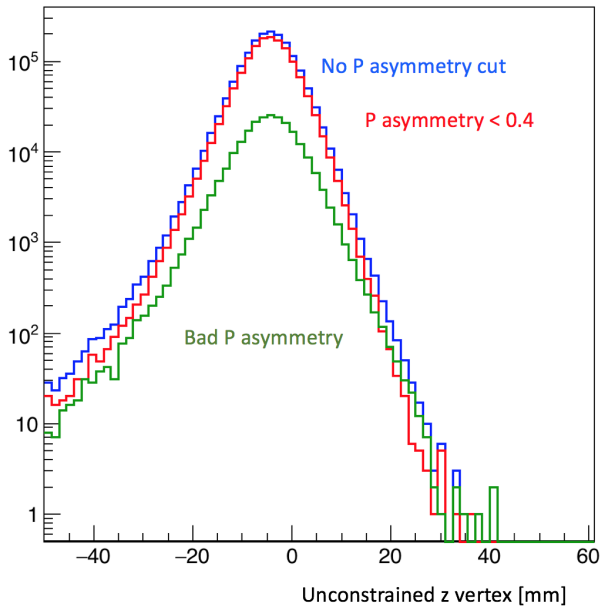

FIG. B.0.6: The effect of the momentum asymmetry (the ratio of the momentum difference to the momentum sum of the two tracks) cut on the tails of the vertex distribution can be seen in the red an green curves.

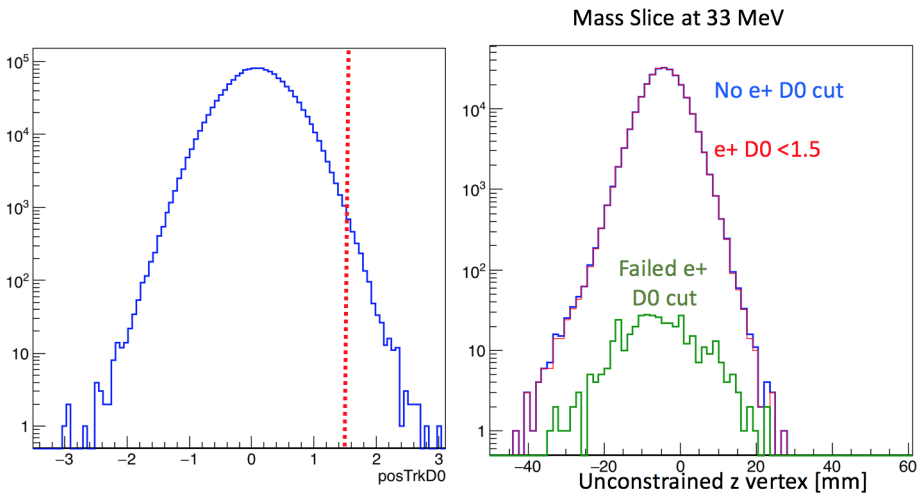

FIG. B.0.7: Positrons that are produced from the photon in wide-angle bremsstrahlung events will have a distance of closest approach that will curve widely at the target location, yielding a largely positive value. The effects of the *DOCA* cut on the vertex distribution is shown here.

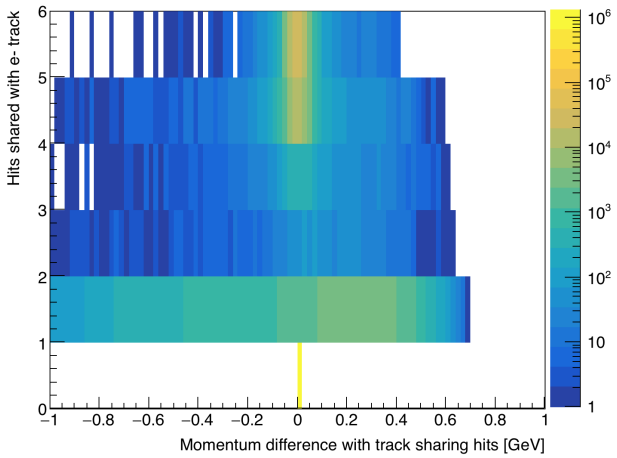

FIG. B.0.8: This plot shows that many of the tracks sharing 4 and 5 hits with the initial track selected in the event have nearly the same momentum.

TABLE 1: Cuts applied to the L1L2 datasets.

Cut type	Cut	Cut Value	%cut	%cut core	%cut tails
track	Fit quality	track $\chi^2 < 30$	38	15	47
track	Max track momentum	$P_{trk} < 75\% E_{beam}$	12	8	14
track	Isolation		11	4	15
vertex	beamspot constraint	bsc$\chi^2 < 10$	46	24	60
vertex	beamspot - unconstrained	bscχ^2-unc$\chi^2 < 5$	20	16	24
vertex	maximum P_{sum}	$< 115\% E_{beam}$	1	1	1
ecal	Ecal SVT matching	$\chi^2 < 10$	7	7	8
ecal	track Ecal timing	< 4ns	5	5	5
ecal	2 cluster time diff	< 2ns	8	6	10
physics	momentum asymmetry	< 0.4	14	15	13
physics	e+ track d0	< 1.5mm	7	3	11
event	max shared hits amongst tracks	< 5 shared hits	8	7	8
track	cuts on kink tails	ϕ and λ kink tails	19	9	36

TABLE 2: Cuts applied to the kinks in layers 1-3.

Cut	Value
Layer 1: ϕ kink, λ kink	¡0.0001,¡0.002
Layer 2: ϕ kink, λ kink	¡0.002,¡0.004
Layer 3: ϕ kink, λ kink	¡0.002,¡0.004

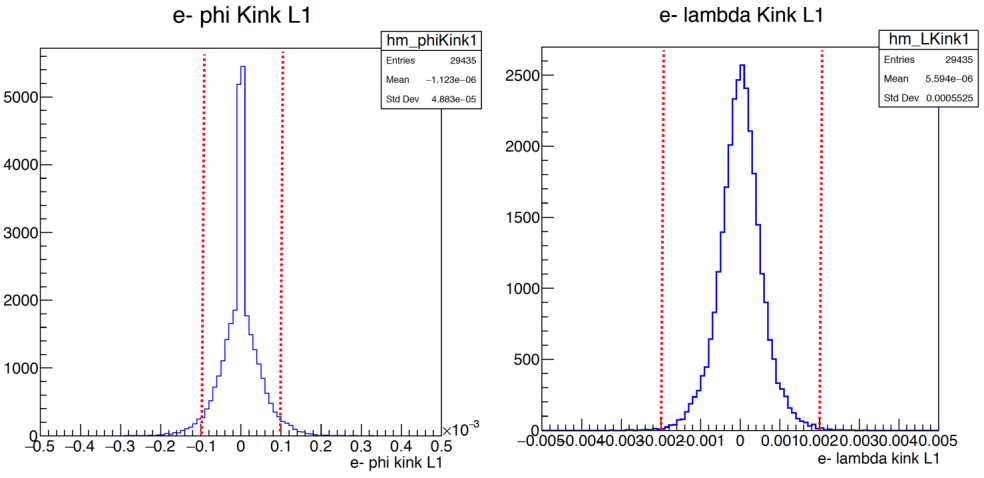

FIG. B.0.9: The kink distributions for tracks passing through Layer 1. The cut is shown at the red dashed line.

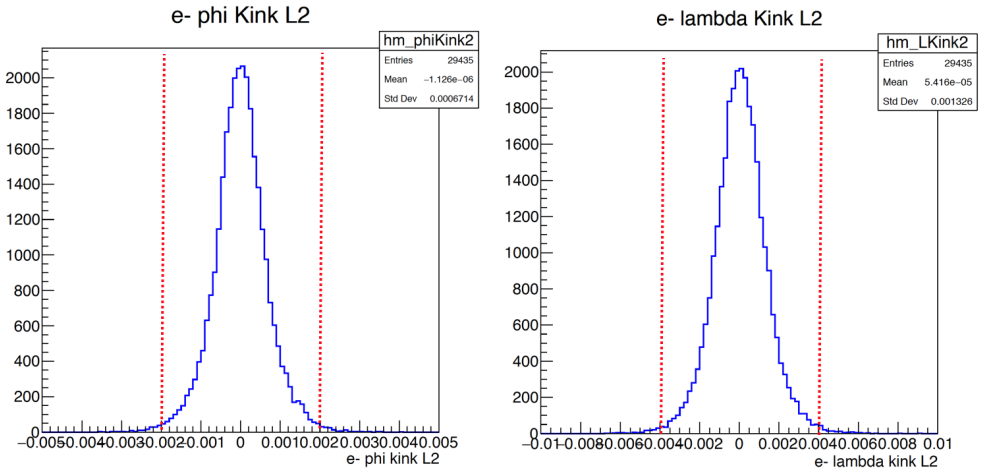

FIG. B.0.10: The kink distributions for tracks passing through Layer 2. The cut is shown at the red dashed line.

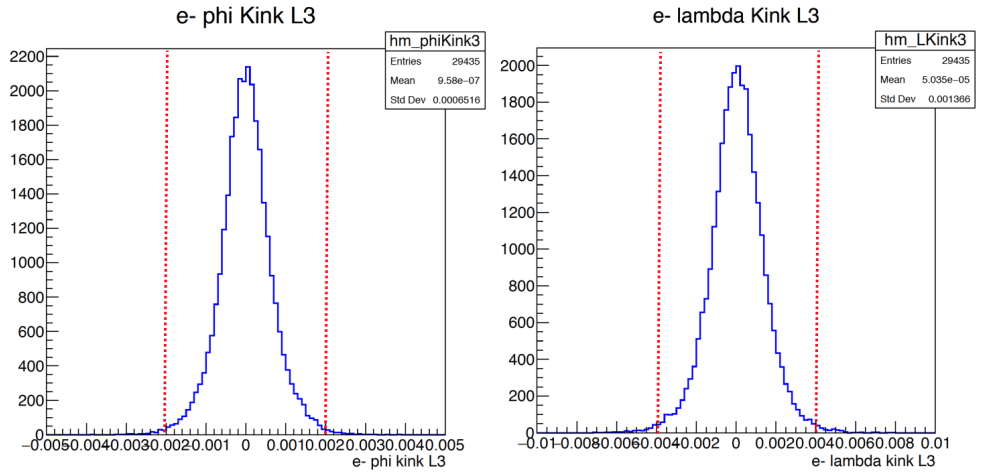

FIG. B.0.11: The kink distributions for tracks passing through Layer 3. The cut is shown at the red dashed line.

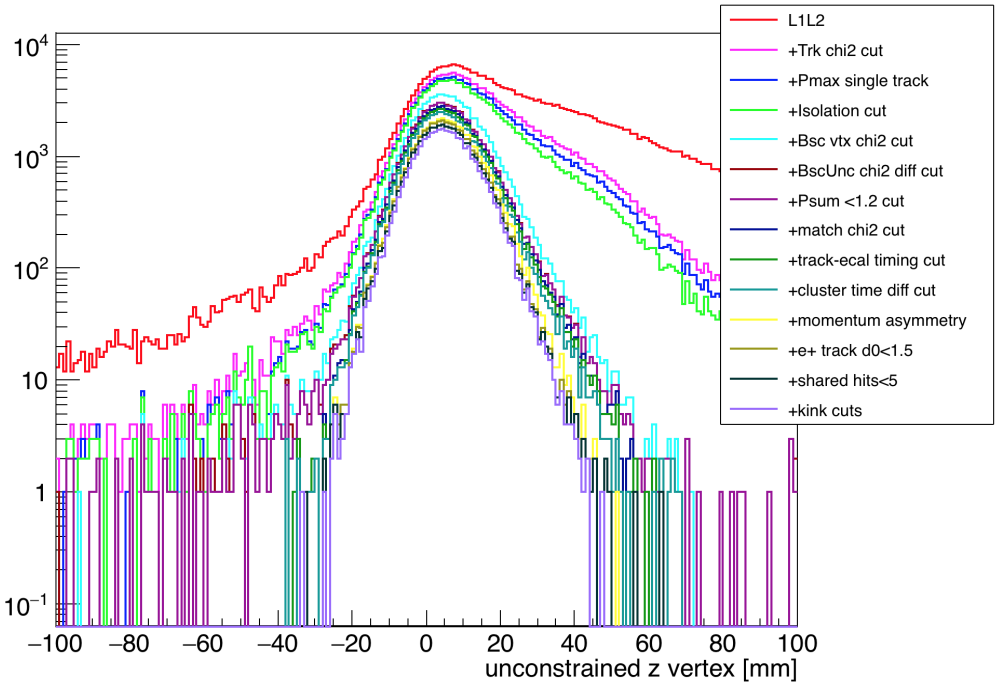

FIG. B.0.12: The effects of the cuts on the L1L2 dataset on the unconstrained z vertex.

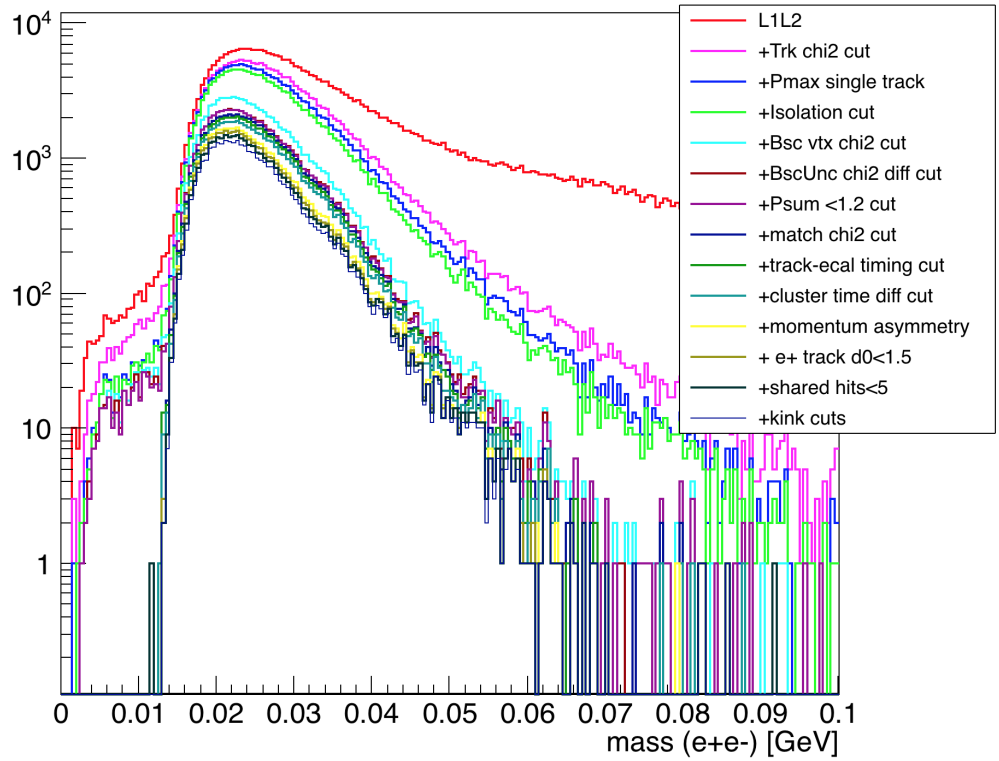

FIG. B.0.13: The effects of the cuts on the L1L2 data set on the mass distribution.

TABLE 3: Cuts applied to the L2L2 data sets.

Cut type	Cut	Cut Value	%cut	%cut core	%cut tails
track	Fit quality	track $\chi^2 < 30$	44	66	44
track	Max track momentum	$P_{trk} < 75\% E_{beam}$	15	14	15
track	Isolation		22	34	22
vertex	beamspot constraint	bsc$\chi^2 < 10$	47	36	47
vertex	beamspot - unconstrained	bscχ^2-unc$\chi^2 < 5$	18	0	19
vertex	maximum P_{sum}	$< 115\% E_{beam}$	1	6	1
ecal	Ecal SVT matching	$\chi^2 < 10$	30	73	29
ecal	track Ecal timing	$<$ 4ns	7	0	8
ecal	2 cluster time diff	$<$ 2ns	8	0	8
physics	momentum asymmetry	< 0.4	4	0	4
physics	e+ track d0	$<$ 1.5mm	21	33	21
event	max shared hits amongst tracks	$<$ 4 shared hits	21	50	21

TABLE 4: Cuts applied to the L1L1 data sets with the SVT at 1.5mm.

Cut type	Cut	Cut Value	%cut	%cut core	%cut tails
track	Fit quality	track $\chi^2 < 30$	37	22	87
track	Max track momentum	$P_{trk} < 75\% E_{beam}$	6	6	19
track	Isolation		2	1	15
vertex	beamspot constraint	bsc$\chi^2 < 10$	23	21	81
vertex	beamspot - unconstrained	bscχ^2-unc$\chi^2 < 5$	12	12	27
vertex	maximum P_{sum}	$< 115\% E_{beam}$	0	0	2
ecal	Ecal SVT matching	$\chi^2 < 10$	3	3	58
ecal	track Ecal timing	$<$ 4ns	5	5	7
ecal	2 cluster time diff	$<$ 2ns	4	4	13
physics	momentum asymmetry	< 0.4	12	12	48
physics	e+ track d0	$<$ 1.5mm	0	0	4
event	max shared hits amongst tracks	$<$ 5 shared hits	12	12	20

TABLE 5: Cuts applied to the L1L2 data sets with the SVT at 1.5 mm.

Cut type	Cut	Cut Value	%cut	%cut core	%cut tails
track	Fit quality	track $\chi^2 < 30$	23	11	47
track	Max track momentum	$P_{trk} < 75\% E_{beam}$	8	7	12
track	Isolation		4	2	10
vertex	beamspot constraint	bsc$\chi^2 < 10$	29	20	62
vertex	beamspot - unconstrained	bscχ^2-unc$\chi^2 < 5$	12	11	22
vertex	maximum P_{sum}	$< 115\% E_{beam}$	0	0	0
ecal	Ecal SVT matching	$\chi^2 < 10$	5	5	7
ecal	track Ecal timing	$<$ 4ns	5	5	5
ecal	2 cluster time diff	$<$ 2ns	6	5	9
physics	momentum asymmetry	< 0.4	14	13	16
physics	e+ track d0	$<$ 1.5mm	6	5	16
event	max shared hits amongst tracks	$<$ 5 shared hits	6	6	6
track	cuts on kink tails	ϕ and λ kink tails	22	8	74

TABLE 6: Cuts applied to the L2L2 data sets with the SVT at 1.5 mm.

Cut type	Cut	Cut Value	%cut	%cut core	%cut tails
track	Fit quality	track $\chi^2 < 30$	29	11	39
track	Max track momentum	$P_{trk} < 75\% E_{beam}$	10	8	12
track	Isolation		5	2	8
vertex	beamspot constraint	bsc$\chi^2 < 10$	26	16	35
vertex	beamspot - unconstrained	bscχ^2-unc$\chi^2 < 5$	10	8	14
vertex	maximum P_{sum}	$< 115\% E_{beam}$	1	1	1
ecal	Ecal SVT matching	$\chi^2 < 10$	11	8	14
ecal	track Ecal timing	$<$ 4ns	6	6	6
ecal	2 cluster time diff	$<$ 2ns	7	6	7
physics	momentum asymmetry	< 0.4	3	2	4
physics	e+ track d0	$<$ 1.5mm	9	7	12
event	max shared hits amongst tracks	$<$ 4 shared hits	20	20	20

APPENDIX C

CONTRIBUTIONS FROM OTHER DATA SETS

The L1L2 data set requires one track to have passed through the active region of Layer 1 with a corresponding hit and the other track to have a first hit in Layer 2. To ensure that a track did not miss Layer 1 due to an inefficiency, the Layer 2 track is extrapolated to Layer 1 and verified that it did not pass through the active region of the silicon sensor. The mass and z vertex distribution for the L1L2 data taken with the SVT at 0.5 mm is shown in Figure C.0.1. The L1L2 data forces the $zCut$ to be very high due to the presence

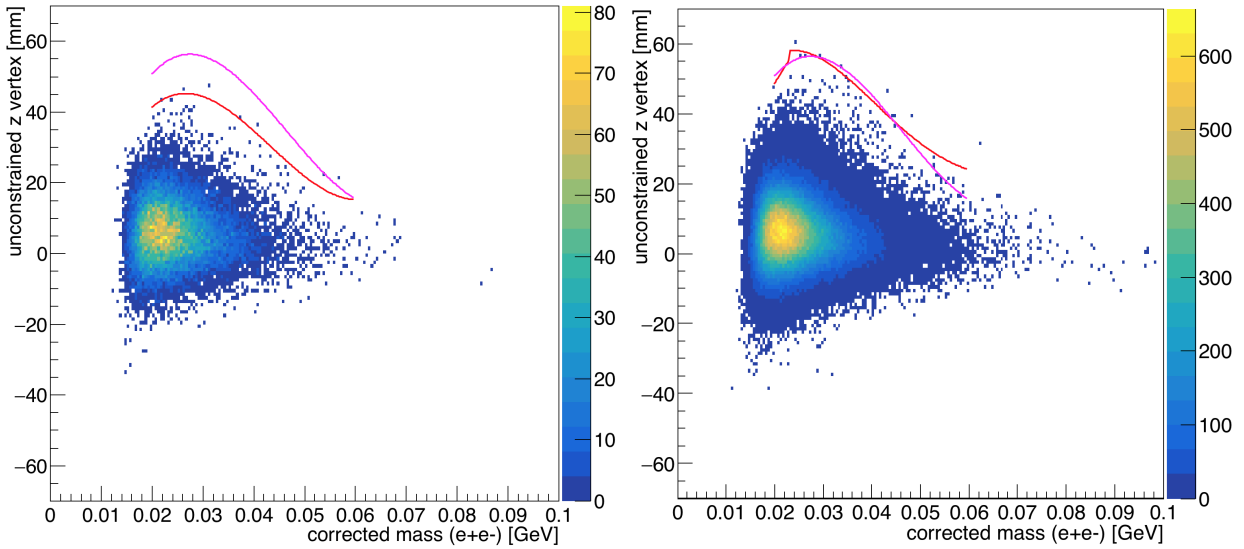

FIG. C.0.1: The unconstrained z vertex position is shown as a function of the corrected mass of the e^+e^- pair where one track has a hit in Layer 1 and the other track does not pass through the active region of Layer 1. The $zCut$ as measured for this data is shown in red and corresponds to the full 100% data set where there is less than 0.5 background event beyond. The projected $zCut$ from the 10% of the data is shown in magenta. The relevant mass range used to measure $zCut$ is from 0.02–0.06 GeV based on measured statistics. The 10% sample for tuning cuts is shown on the left, and the full 100% of the data is shown on the right.

of a large high z background component. WAB conversions in Layer 1 generally have an electron in Layer 1 and the positron track in Layer 2 (missing Layer 1). This accounts for most of the statistics of this data. However, even if the data is divided for events where the electron has a hit in Layer 1 and the positron has a hit in Layer 1, there are still large high

z backgrounds for each set. No one vertex cut (such as on the beam spot constraint quality) is able to remove these events. The measured $zCut$ for this data set is so large that the data cannot contribute to the reach. A significantly lower $zCut$ could restore some of the reach from this set, but the reach obtained is still much less than L1L1 data set.

The mass and z vertex distribution for the L1L2 data taken with the SVT at 1.5 mm is shown in Figure C.0.2. This data has significantly fewer high z background events than that

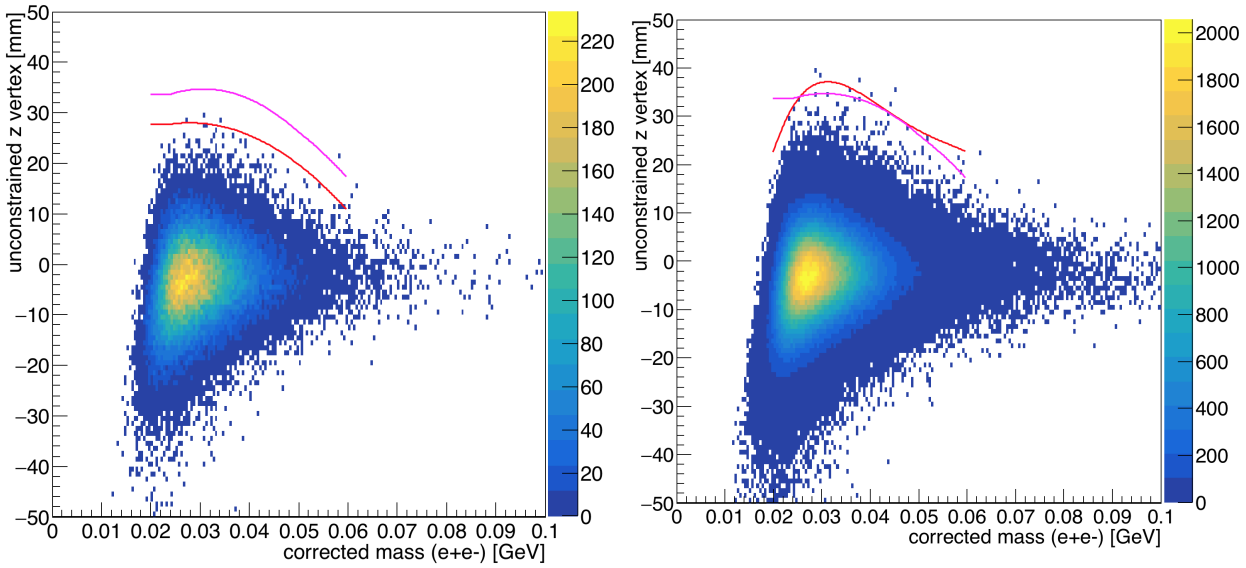

FIG. C.0.2: The unconstrained z vertex position is shown as a function of the corrected mass of the e^+e^- pair where one track has a hit in Layer 1 and the other track does not pass through the active region of Layer 1. The $zCut$ as measured for this data is shown in red and corresponds to the full 100% data set where there is less than 0.5 background event beyond. The projected $zCut$ from the 10% of the data is shown in magenta. The relevant mass range used to measure $zCut$ is from 0.02–0.06 GeV based on measured statistics. The 10% sample for tuning cuts is shown on the left, and the full 100% of the data is shown on the right.

shown in Figure C.0.1.

The L2L2 data sets are composed of vertexed pairs of tracks that missed Layer 1 and extrapolate to the outside of the active region of the silicon sensor in Layer 1. The mass and z vertex distribution for the L2L2 data taken with the SVT at 0.5 mm is shown in Figure C.0.3. The L2L2 data with the SVT at ± 0.5 mm from the beam is dominated by high z backgrounds. This background appears to go all the way out to the first SVT layer. Due to this background alone, this data set cannot contribute to the projected reach. Ideally, there should be no events in this data set except for pure signal events. These events cannot be signal due to their uniform distribution over several masses. A $zCut$ should be able to

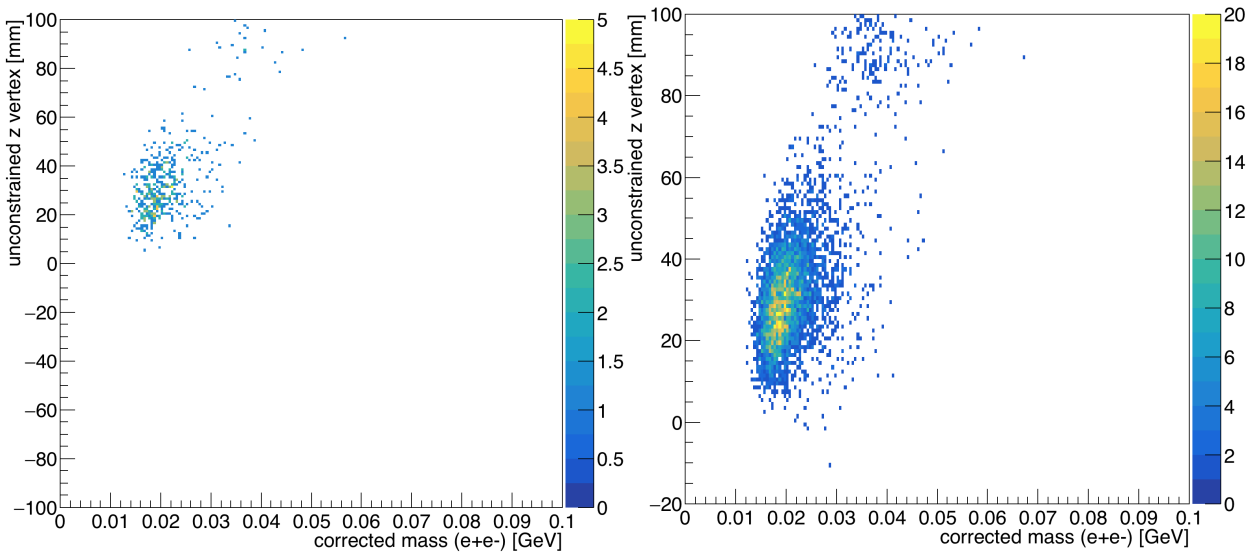

FIG. C.0.3: The unconstrained z vertex position is shown as a function of the corrected mass of the e^+e^- pair where both tracks do not pass through the active region of Layer 1. The $zCut$ as measured for this data is shown in red and corresponds to the full 100% data set where there is less than 0.5 background event beyond. The projected $zCut$ from the 10% of the data is shown in magenta. The relevant mass range used to measure $zCut$ is from 0.02–0.06 GeV based on measured statistics. The 10% sample for tuning cuts is shown on the left, and the full 100% of the data is shown on the right.

be chosen for this data such that the reconstructed vertex efficiency can be optimized, but this is only true if the background events can be removed.

The L2L2 data with the SVT slightly more open at ±1.5 mm from the beam is shown in Figure C.0.4. The mass and z vertex distribution for the L2L2 data taken with the SVT at 1.5 mm is shown in Figure C.0.4. The L2L2 data at 1.5 mm has considerably fewer high z background events than the data from 0.5 mm. While a $zCut$ for this data can be obtained, the statistics of the 1.5 mm data set are too low to obtain additional reach contributions.

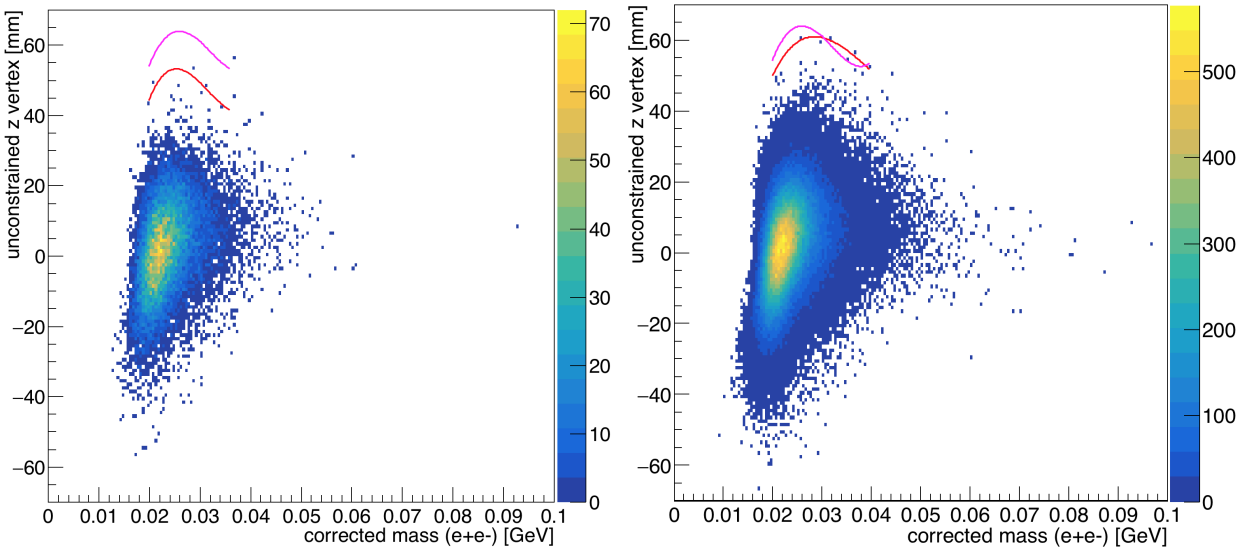

FIG. C.0.4: The unconstrained z vertex position is shown as a function of the corrected mass of the e^+e^- pair where both tracks do not pass through the active region of Layer 1. The $zCut$ as measured for this data is shown in red and corresponds to the full 100% data set where there is less than 0.5 background event beyond. The projected $zCut$ from the 10% of the data is shown in magenta. The relevant mass range used to measure $zCut$ is from 0.02–0.04 GeV based on measured statistics. The 10% sample for tuning cuts is shown on the left, and the full 100% of the data is shown on the right.

VITA

Holly Szumila-Vance
Department of Physics
Old Dominion University
Norfolk, VA 23529

Education:

Old Dominion University, Norfolk, VA

- PhD Candidate in experimental nuclear physics, 2012–2017
- Master of Science, 2014

Embry–Riddle Aeronautical University, Prescott, AZ

- Bachelor of Science in Aerospace Engineering, 2009
- Bachelor of Science in Space Physics, 2008

Research Experience:

- 2013–2017, graduate research assistant searching for heavy photons in the Heavy Photon Search experiment at Jefferson Lab, Hall B
- 2013, graduate research assistant testing CLAS12 Region II drift chambers at the Old Dominion University clean room

Publications:

- N. Baltzell, et al, "The HPS beamline and its performance", Nucl. Inst. And Meth. A, in press; https://arxiv.org/pdf/1612.07821.pdf
- I. Balossino, et al.,"The HPS electromagnetic calorimeter, Nucl. Inst. And Meth. A, in press; https://arxiv.org/pdf/1610.04319v2.pdf

Previous Work Experience:

- Old Dominion University: Astronomy teaching assistant
- Virginia Army National Guard: Assistant S-3, operations officer
- Arizona Army National Guard: MEDEVAC platoon leader
- Center for Space Nuclear Research, research internship

Typeset using LaTeX.